scientific reports

Check for updates

OPEN

Immunological and structural evaluation of the intranasally administrated CVB1 whole-virus and VLP vaccines

Saana Soppela[1], Zlatka Plavec[2], Stina Gröhn[1], Iiris Mustonen[1], Minne Jartti[1], Sami Oikarinen[3], Mira Laajala[4], Varpu Marjomäki[4], Sarah J. Butcher[2] & Minna M. Hankaniemi[1]✉

Coxsackievirus B1 (CVB1) is a common cause of acute and chronic myocarditis, cardiomyopathy, and meningitis. CVBs replicate in mucosal membranes. Therefore, vaccines inducing robust mucosal immune responses are needed. We investigated the immunogenicity of virus-like particles (VLP) and inactivated virus vaccines for CVB1, administered to mice either subcutaneously or intranasally, formulated with and without commercial and an experimental adjuvant. In this study, epigallocatechin-3-gallate (EGCG) was used both as a potential adjuvant and as an inactivating agent. EGCG adjuvanted CVB1-VLP enhanced immunogenicity via the parenteral route, but not intranasally. EGCG-adjuvanted and non-adjuvanted CVB1-VLPs triggered an immune response after intranasal administration, although the response remained weak. Intranasal administration of formalin-inactivated virus elicited robust CVB1-specific humoral, cellular, and mucosal immune responses, but after EGCG-inactivation, the mucosal antibody response was lower than after formalin-inactivation. To identify the link between structure and mucosal immunogenicity, we solved the structures of CVB1-VLP and formalin-inactivated CVB1 virus at resolutions ranging from 2.15 to 4.1 Å. The structural difference between VLP and formalin-inactivated CVB1 was the presence of the genome and cross-linked amino acid residues in the formalin-inactivated virus. Formalin-inactivated CVB1 vaccine shows promise for mucosal immunizations and the structural data supports the development of next-generation VLP-vaccines in the future.

Coxsackieviruses B (CVBs) are classified within the *Enterovirus B* species and include six distinct serotypes (CVB1-CVB6) (https://ictv.global/report/chapter/picornaviridae/picornaviridae/enterovirus accessed 6.3.2024). Besides common cold symptoms, CVB infection can lead to severe outcomes especially in immunocompromised individuals. These complications may manifest for instance as meningitis[1], pancreatitis[2], and myocarditis[3].

Mature CVB1 virions, like other enteroviruses, have four structural proteins termed viral protein 1–4 (VP1-4)[4,5]. They form an icosahedrally-symmetric capsid of about 30 nm in diameter with VP1 around the 5-folds, VP2 either side of the 2-folds and alternating VP2 and VP3 around the 3-fold symmetry axes[4,5]. VP1-3 fold as β-sheet jelly-rolls[4–6]. VP4 spans the inside of the capsid below the 5-fold and is embraced by VP1 N-terminal arms[4,5]. At the base of VP1, there is a hydrophobic pocket which normally contains a lipid factor[4,5]. During virion maturation, cleavage of the precursor protein VP0 to VP2 and VP4 occurs, a process catalyzed by RNA[7]. In addition to the virion, two alternative CVB1 capsids have been described, the A-particle and the empty particle. A-particles can form from the virion when CVB1 interacts with a host receptor[5]. The A-particles are characterized by 4% expansion, formation of pores in the capsid, collapse of the hydrophobic pocket that held the lipid factor and loss of VP4[5], allowing for the exit of the genome into the host cell. Empty particles can have the virion or A-particle conformation but lack RNA[5,8].

[1]Virology and Vaccine Immunology, Faculty of Medicine and Health Technology, Tampere University, Tampere, Finland. [2]Faculty of Biological and Environmental Sciences, Molecular and Integrative Bioscience Research Programme, & Helsinki Institute of Life Sciences-Institute of Biotechnology, University of Helsinki, Helsinki, Finland. [3]Medical Virology, Faculty of Medicine and Health Technology, Tampere University, Tampere, Finland. [4]Department of Biological and Environmental Science/Nanoscience Center, University of Jyväskylä, Jyväskylä, Finland. ✉email: minna.hankaniemi@tuni.fi

Similar to empty particles, recombinantly produced virus-like particles (VLPs) closely mimic the structure of infectious viruses but lack RNA. CVB1 VLPs self-assemble from viral capsid proteins, forming an icosahedral structure resembling native virions. Production processes for VLPs exhibit rapid scalability compared to traditional culture methods[9,10] and VLP vaccines can be generated for virus strains that do not readily grow in cell cultures. However, VLPs may lack equally robust immunogenicity of their virus-based counterparts and typically require the use of adjuvants for enhanced efficacy. Moreover, these VLPs may differ from native viruses in terms of antigenic properties, due to differences in protein structure, post-translational modifications, and the presence of the viral genome.

Formalin inactivation of viruses is important in the commercial production of human vaccines. When we applied an optimized formalin inactivation protocol[11] in the production of a novel hexavalent vaccine targeting the six known CVB serotypes, we showed that the vaccine has excellent safety and immunogenicity profiles in murine models and nonhuman primates[12]. However, treating the CVB1 virus too long with formalin, causes capsid disintegration with subsequent decrease of the virus concentration[11]. Also, we have shown that UV treatment destabilizes CVB1 virus[13] and CVB1-VLP[14] at elevated temperatures and lowers the immunogenicity of the vaccines, demonstrating the importance of treating the particles without destroying the conformation of the particle and the immunogenic epitopes. Although, our preclinical studies with CVB1-[14] and CVB3-[15] VLPs have shown that these VLPs can induce high neutralizing and total IgG antibody levels, primarily of a Th2 type phenotype in the sera of immunized mice, additional ancillary components inducing mucosal immunity are also needed.

Here, we studied the potential of a known enterovirus capsid binding antiviral compound epigallocatechin-3-gallate (EGCG) as a vaccine adjuvant. EGCG is a type of catechin, a polyphenolic molecule abundant in green tea and it has been previously studied as a potential antiviral agent[16–21] and an adjuvant in a vaccine formulation[22]. EGCG significantly inhibits viral replication of hepatitis C[16,17], hepatitis B[18], influenza[19,20] and enterovirus-71[21]. Recently it has also been shown to have antiviral properties against enteroviruses such as CVB1, CVB3 and CVA9[23]. Additionally, EGCG has been studied as a vaccine adjuvant, enhancing the efficacy of an influenza subunit vaccine by inducing high levels of neutralizing antibodies, like the adjuvant alum[22]. In addition to EGCG, we also tested a known adjuvant system 04 (AS04) that contains aluminium hydroxide and 3-O-desacyl-4′-monophosphoryl lipid A (MPLA) and is currently used in approved vaccines[24].

The route of immunization affects the protective efficacy of vaccines and since mucosal sites are primary access points for CVBs, the induction of mucosal immunity by vaccination may prevent pathogen entry, infection and disease. According to our knowledge, no preclinical studies demonstrating the immunogenicity and safety of CVB1-VLP and inactivated CVB1 virus vaccines via the intranasal route have been published. Here, we demonstrate for the first time that CVB1-VLP elicited a weak but detectable immune responsewhen administrated intranasally without adjuvants and that formalin-inactivated CVB1 is a promising mucosal vaccine for future clinical use. Based on the atomic resolution structures determined here for the CVB1-VLP and formalin-inactivated CVB1 virus, we can further develop next-generation VLP-based vaccines targeting enteroviruses in the future. Graphical abstract summarizing the main finding of the study can be seen in Fig. 1.

Results

Characterization of $VLP_{No-Tween80}$ and $VLP_{Tween80}$ and binding capacity of EGCG to the VLPs

Our previous studies have demonstrated that the use of Tween80 during purification significantly enhances the stability and yield of CVB1 and CVB1-VLP preparations[11,13,14]. Given EGCG's antiviral properties in the absence of Tween80[21], separate VLP preparations were purified using previously established purification method[14] and were stored without and with Tween80 (designated $VLP_{No-Tween80}$ and $VLP_{Tween80}$). VLP purification in the presence of Tween80 led to 5.2 times better pure protein yield compared to preparation in its absence (11.4 mg/L pure $VLP_{Tween80}$ and 2.2 mg/L pure $VLP_{No-Tween80}$). SDS-PAGE analysis and densitometric analysis confirmed the purity of the VLPs, resulting in ≥ 95% pure preparations for $VLP_{No-Tween80}$ (Fig. 2A, Supplementary Fig. 1A) and for $VLP_{Tween80}$ (Fig. 2B, Supplementary Fig. 1B). Electron micrographs of negatively-stained preparations showed intact particles with an average particle size of 30 nm (Fig. 2C and D). Subsequently, we determined the stability of the VLPs at room temperature (RT) as well as the binding capacity of the antiviral compound, EGCG, to the VLPs in the absence and in the presence of Tween80. DLS analysis of the freshly prepared $VLP_{No-Tween80}$ showed a homogeneous monodisperse distribution, 100% of the particles had an average hydrodynamic diameter of 29.1 nm (± 0.44) (Fig. 2E). However, stability testing over 120 h in Tris-buffer at RT revealed particle aggregation, with 30.9% (± 2.4) of $VLP_{No-Tween80}$ particles aggregating after 48 h, representing an average particle population of 829 (± 29.25) nm in diameter and 54.6% (± 0.1) of $VLP_{No-Tween80}$ particles had aggregated after 120 h, representing an average particle population of 1021 (± 11.58) nm in diameter (Fig. 2E). Also, $VLP_{Tween80}$ was analyzed for stability with DLS. Measurement immediately, after 120 h and after one month showed that the average hydrodynamic diameter of 28.13 nm (± 0.62) that was first measured from 100% (± 0.3), did not change significantly (Fig. 2F). This demonstrated that purification with Tween80 significantly improved the solubility and stability of CVB1-VLP.

DLS was exploited in determining EGCG's binding capacity to the VLPs. DLS analysis demonstrated that 100% of $VLPs_{No-Tween80}$ immediately agglomerated in the presence of EGCG, resulting in an average hydrodynamic diameter of 1714 nm ± 154.4 (Fig. 2G). However, after 24 h incubation at RT, 96.7% (± 0.26) the average particle population size had reduced to 30.6 (± 0.82) nm in diameter (Fig. 2G). After 48 h, the $VLP_{No-Tween80}$ particle population was like the VLP samples incubated without EGCG, indicating time-dependent and reversible binding of EGCG to CVB1-VLP particles that do not contain Tween80 (Fig. 2E and G). Furthermore, DLS analysis revealed that EGCG caused measurable agglomeration of $VLP_{Tween80}$ from 0 to 24 h, with particle detachment from the agglomerate occurring after 48 h, when 91.8% (± 3.4) of $VLP_{Tween80}$ particles had an average hydrodynamic diameter of 27.1 nm (± 1.45) (Fig. 2H).

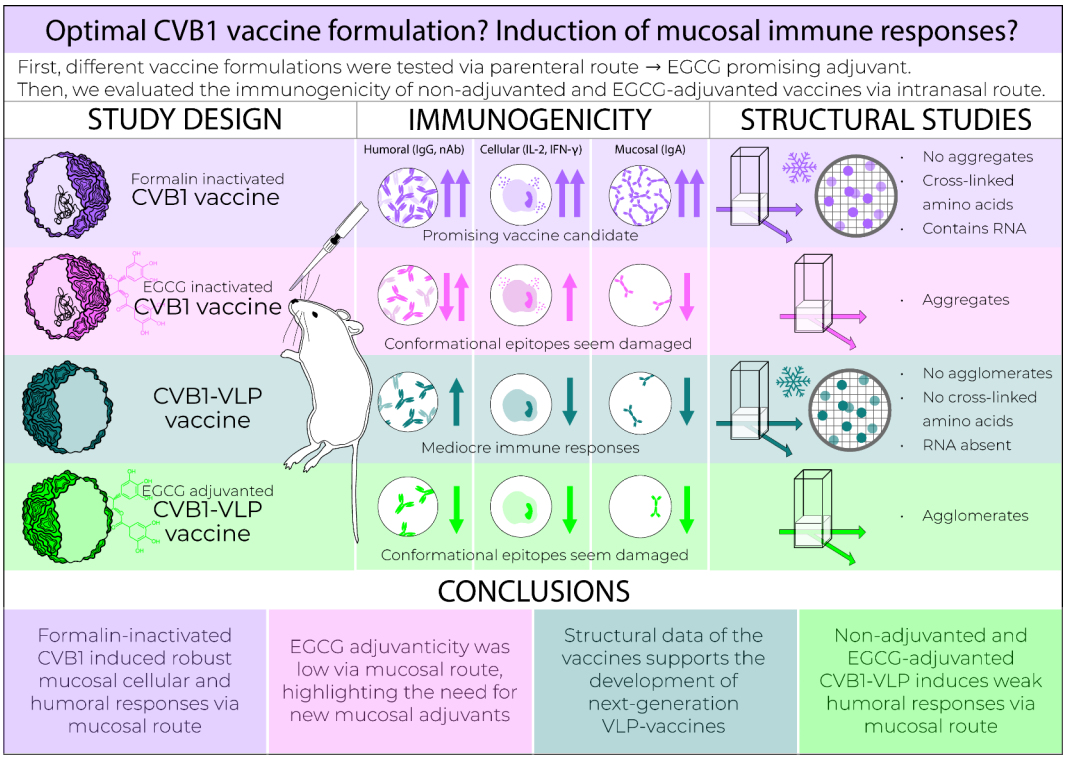

Fig. 1. Graphical abstract summarizing the main findings of the study.

EGCG functions as potential vaccine adjuvant for CVB1-VLP via parenteral immunization route

First, we assessed the immunogenicity of the CVB1-VLP$_{\text{No-Tween80}}$ administrated *via* the subcutaneous immunization route. This formulation was used to evaluate the immune response elicited by the VLP in its pure form, without the potential structural or immunological influence of Tween80. We compared the humoral immune response of CVB1-VLP$_{\text{No-Tween80}}$ in combination with the well-established parenteral adjuvant system 04 (AS04) or with the potential adjuvant EGCG (Fig. 3). Formalin-inactivated whole-virus vaccine was included as a reference vaccine, that has previously been demonstrated to induce robust immune responses when administrated parenterally[11–13,25,26]. The 2 µg dose was selected based on previous titration study[14] and to allow for a more direct comparison with our previous work on formalin-inactivated CVB1[11].

The highest levels of antigen-specific IgG antibodies were observed in the sera of CVB1-VLP$_{\text{No-Tween80+AS04}}$ group (Fig. 3B). Interestingly, IgG1 antibody titers were most noticeable in mice sera immunized with CVB1-VLP$_{\text{No-Tween80+EGCG}}$, suggesting a potential enhancement of the antigen-specific humoral immune responses by EGCG (Fig. 3C). CVB1-VLP$_{\text{No-Tween80+EGCG}}$ exhibited the least variance in neutralizing antibody titers against CVB1, as seen in Fig. 3E. The sensitivity between the ELISA and neutralization assays differs remarkably, because ELISA can detect antigen-specific low-affinity IgG binding, whereas the neutralization assay requires a higher concentration of functionally active antibodies to achieve measurable virus neutralization.

Furthermore, mice in all the vaccine groups were healthy as the weight gain continued as expected (Fig. 3F). The IgG1/IgG2a ratio for the formalin-inactivated CVB1 group was 0.81 indicating balanced response whilst all VLP groups had strongly Th2 biased ratio with 18.7 for VLP$_{\text{No-Tween80}}$, for 5.11 for VLP$_{\text{No-Tween80+AS04}}$, and notably 109.6 for VLP$_{\text{No-Tween80+EGCG}}$. Due to ethical considerations, the number of animals used in the pilot study was low, and the results had no clear statistical significance. The study demonstrated that EGCG appears to induce a pronounced Th2 bias in the immune response. The results from the pilot animal study supported the usage of EGCG as a potential vaccine adjuvant and based on these results, we decided to further study the applicability of EGCG in CVB1 virus inactivation and as a mucosal adjuvant.

Characterization of EGCG inactivated CVB1 virus vaccine candidate

Although formalin inactivated viruses are in wide use in clinical vaccines, formalin inactivation has been shown to cause destruction of some immunogenic epitopes compared to live vaccines[11,28]. Therefore, we tested inactivation of CVB1 using EGCG incubation as a potential replacement for formalin (Fig. 4). Dynamic light scattering (DLS) analysis of active CVB1 virus revealed that the virus can be stored at room temperature (RT) up to 1 month without significant change in the average particle diameter, volumetric distribution or infectivity. At day 0, 92% (± 1.2) of virus-particles had an average hydrodynamic diameter of 30.7 nm (± 3.28) whereas after 1 month storage in RT, 91.1% (± 2.0) of the particles had an average hydrodynamic diameter of 33.4 nm (± 1.6) (Fig. 4A).

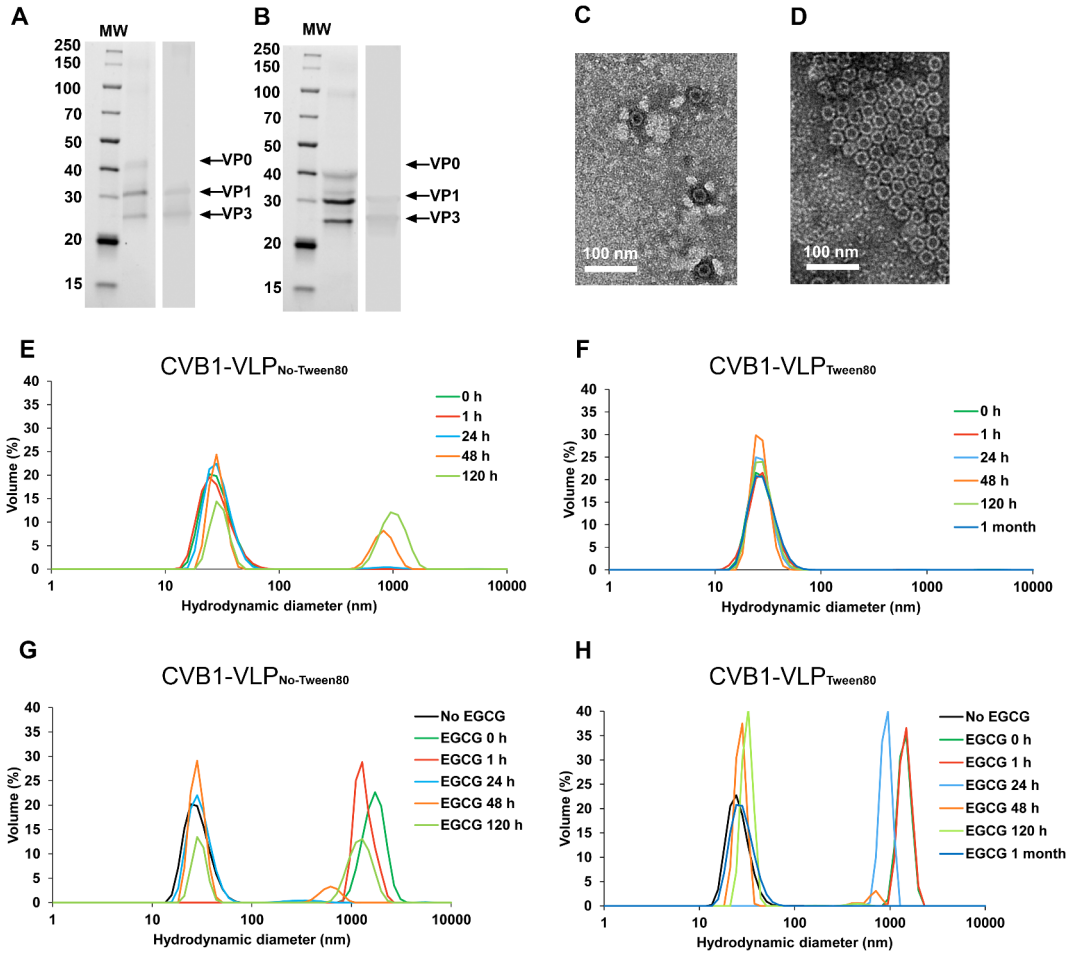

Fig. 2. CVB1-VLP$_{No-Tween80}$ and CVB1-VLP$_{Tween80}$ characterization, stability and binding capacity to EGCG. SDS-PAGE and Western Blotting of purified (**A**) CVB1-VLP$_{No-Tween80}$ and (**B**) CVB1-VLP$_{Tween80}$. The left panel in **A** and **B** shows the stainfree total protein staining of the purified CVB1-VLP$_{No-Tween80}$ and CVB1-VLP$_{Tween80}$. In the right panels of **A** and **B** VP1 and VP3 capsid proteins were detected by Western blot stained with a polyclonal anti-CVB1-6 rabbit antibody. VLP capsid proteins are indicated with arrows. **B**) Transmission electron micrographs of the negatively-stained purified (**C**) VLP$_{No-Tween80}$ and (**D**) CVB1-VLP$_{Tween80}$ with 25 000x magnification. Dynamic Light Scattering (DLS) analysis of (**E**) CVB1-VLP$_{No-Tween80}$ and (**F**) CVB1-VLP$_{Tween80}$ stored at room temperature. DLS analysis of (**G**) CVB1-VLP$_{No-Tween80}$ and (**H**) CVB1-VLP$_{Tween80}$ incubated with EGCG at room temperature.

DLS analysis of CVB1 incubated with EGCG at RT showed immediate aggregation of the virus, and this seemed to be irreversible as the measurement result did not change after one month (Fig. 4B). However, based on infectivity measurement with a $TCID_{50}$ assay, CVB1 was only completely inactivated by EGCG after one month incubation at RT, a result achieved by formalin inactivation after only 5 days (Fig. 4C). The infectivity titer of CVB1 stored for 1 month at RT decreased from 9.67×10^{11} to 2.59×10^{7} TCID50 units/ml (Fig. 4C), demonstrating that EGCG is needed to inactivate the virus. Our next objective was to evaluate the immunogenicity of EGCG inactivated CVB1 virus and CVB1-VLP with EGCG as an adjuvant via the intranasal immunization route.

Formalin inactivated CVB1 induces robust immunogenicity via intranasal immunization route

We compared the immunogenicity of formalin and EGCG inactivated CVB1 vaccines ($CVB1_{EGCG}$ and $CVB1_{Formalin}$) to CVB1-VLP$_{Tween80}$ alone or formulated with EGCG (CVB1-VLP$_{Tween80+EGCG}$) when administrated via intranasal immunization (Fig. 5A). To evaluate mucosal immune responses, bronchoalveolar lavages (BAL) were collected from the mice at the termination of the study. The antigen-specific IgA and IgG significantly increased in the $CVB1_{Formalin}$ group in contrast to the low responses in the $CVB1_{EGCG}$ group (Fig. 5B-D). A similar trend was seen in the CVB1 neutralizing antibodies from BAL samples, although no statistical significance was obtained. CVB1-VLP groups elicited low or negligible mucosal responses, as illustrated in Fig. 5B-D. Cellular immunogenicity (IFN-γ, IL-2, and TNFα secretion levels) induced by the vaccines was measured from splenocytes extracted from the vaccinated animals and stimulated with active CVB1. Interestingly, $CVB1_{Formalin}$ and $CVB1_{EGCG}$ groups demonstrated heightened cytokine secretion patterns compared to CVB1-VLP groups

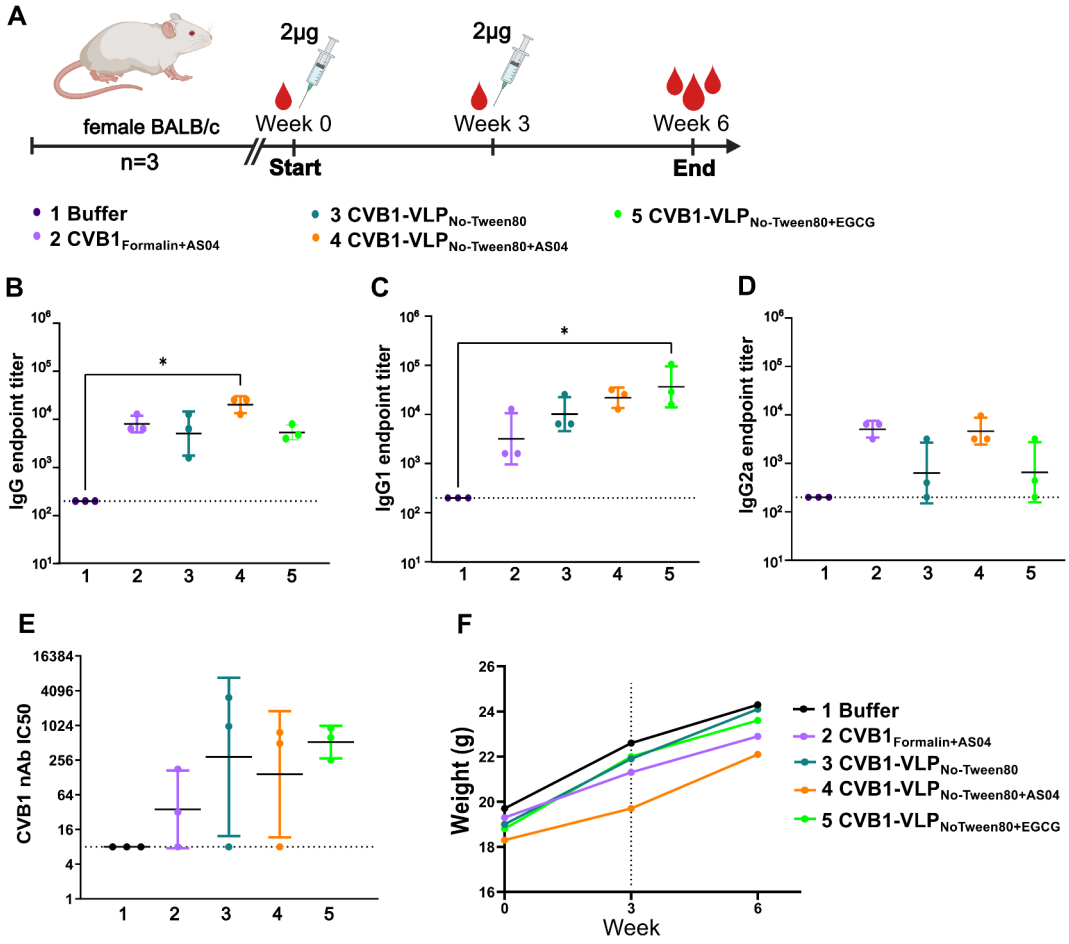

Fig. 3. Pilot animal study. (**A**) Immunization schedule. (**B**) Vaccine antigen-specific IgG, (**C**) IgG1 and (**D**) IgG2a antibody end point titers at week 6 after two subcutaneous immunizations with 2 µg vaccine antigen determined with indirect ELISA. Titers below 200 were assigned as negative result. (**E**) CVB1 neutralizing antibodies determined with microneutralization assay. Titers below 8 were assigned as a negative result. A-E). Data is shown as geometric mean with geometric SD. (**F**) Average weights of animals in each experimental group. Dashed line indicates the time point for booster vaccination. * = $p < 0.05$.

that displayed limited cellular responses (Fig. 5E-G). While EGCG appeared to increase cytokine secretion in some animals, there was greater variability among animals in the EGCG-inactivated group compared to the formalin-inactivated virus group.

Neutralizing antibodies, antigen-specific IgG, and IgG subtypes IgG1 and IgG2a were quantified from the termination serum. The $CVB1_{Formalin}$ group exhibited significantly higher responses across all antibody types (Fig. 5H-K), with an average IgG1/IgG2a ratio of 0.20. This ratio indicates a slightly Th1-biased immune response. On the contrary, $CVB1_{EGCG}$ elicited a weak neutralizing antibody response and a diminished IgG1 response, suggesting inhibition of humoral immune response. Despite this, the average IgG1/IgG2a ratio in this group was 0.59 with modest improvement in the IgG2a antibody response, aligning with the observed cytokine secretion patterns of the $CVB1_{EGCG}$ group. Compared to the $CVB1_{Formalin}$, the $CVB1\text{-}VLP_{Tween80}$ group elicits a mediocre humoral immune response, indicating that VLPs undergo antigen processing from the mucosa but not as efficiently as the $CVB1_{Formalin}$. Furthermore, $CVB1\text{-}VLP_{Tween80+EGCG}$ inhibited the VLP intake compared to $CVB1\text{-}VLP_{Tween80}$. Both VLP groups had a Th2-biased immune response with IgG1/IgG2a ratios being 3.42 for $CVB1\text{-}VLP_{Tween80}$ and 112.7 for $CVB1\text{-}VLP_{Tween80+EGCG}$. These results suggest that EGCG does not enhance mucosal antigen intake; rather, it diminished it. On the contrary, formalin inactivated CVB1 without added adjuvants raised a balanced immune response both mucosally and systemically, when administrated intranasally.

CryoEM analysis of $CVB1\text{-}VLPs_{Tween80}$ and $CVB1_{formalin}$

To further understand the immunogenic differences between the preparations, we examined the structures of the $CVB1\text{-}VLP_{Tween80}$ particles and $CVB1_{formalin}$ preparations used in intranasal vaccinations (Fig. 5). 13 860 micrographs of $CVB1\text{-}VLP_{Tween80}$ were collected and 226 223 particles were picked (Table 1; Fig. 6A, B). Through classification steps, particles were later separated into 2 distinct classes, compact $CVB1\text{-}VLP_{Tween80}$ structurally corresponding to native CVB1 virions with VP0, 1 and 3 (PDB ID 7DPF) and expanded, $CVB1\text{-}VLP_{Tween80}$ similar to CVB1 A-particles (PDB ID 7DQ4, Table 1; Figs. 6C and F-I and 7A-C, E and F)[5]. The

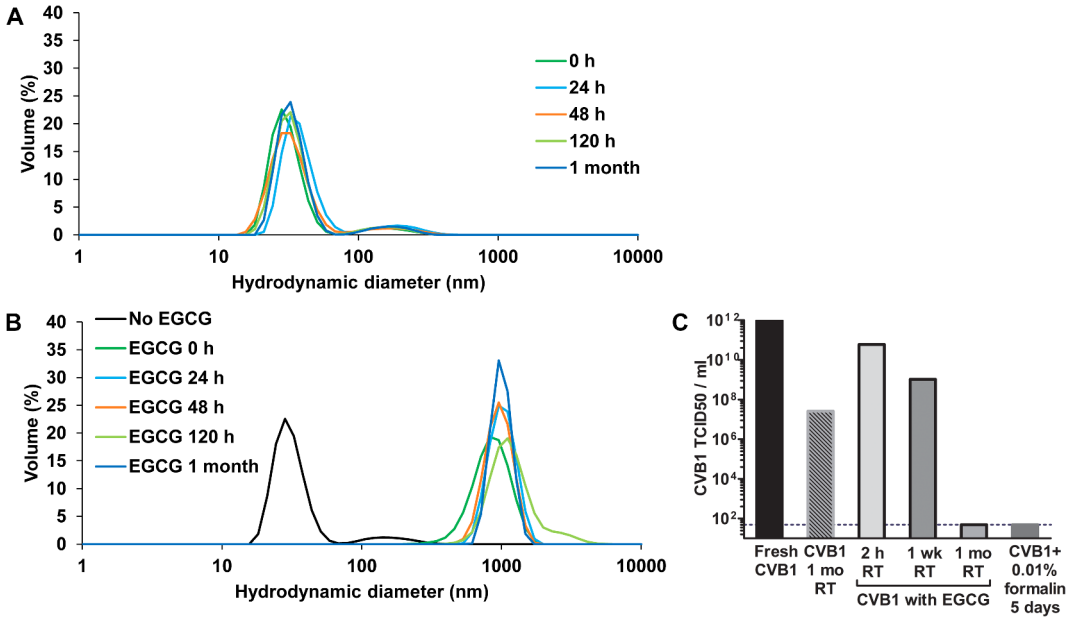

Fig. 4. Characterization of CVB1 virus. (**A**) DLS analysis of purified CVB1 virus stored at room temperature (RT) for 1 month. (**B**) DLS analysis of purified CVB1 virus incubated with EGCG at RT for 1 month. (**C**) To confirm that the virus was inactivated with EGCG and unable to replicate, $TCID_{50}$-assay was carried out.

particle distribution was 48–52% in favor of the expanded particles (Table 1). Particle sets were processed in cryoSPARC and Scipion to 2.15 Å resolution (Table 1; Fig. 6D, E,H, I). The high resolution and quality of the reconstructed data can be observed in Fig. 7H and Supplementary Fig. 2A. At the current resolution, an ion coordinated between three D203 at the 3-fold (Fig. 6H) can be observed in both expanded and compact forms. In the expanded CVB1-$VLPs_{Tween80}$, a forked density is present above cysteins which could be additional ion densities and in the compact CVB1-$VLP_{Tween80}$ two conformations of VP3 R232 are resolved (Supplementary Fig. 2A). Local resolution estimation gives the lowest resolution of 2.44 Å at the flexible regions on the sides of the 2-folds outside and inside the capsid (Fig. 6H, I).

Compact CVB1-$VLP_{Tween80}$ density map fits well the model of native mature CVB1 taken from PDB ID: 7DPF (Fig. 7A-E, H)[5]. The structure and position of VP0 in VLPs corresponds to VP2 and VP4 in mature virions, however lacking a 39 residues-long section on the inside of the capsid, the N-terminus and myristoyl group (Table 1; Fig. 7A). Furthermore, N-terminal arms embracing the VP4 in the native CVB1 could not be modelled prior to residue 56 in the CVB1-$VLP_{Tween80}$ (Table 1; Fig. 7E). Other characteristic structural features of native CVB1 are seen, such as the VP1 around the 5-fold (Fig. 7A), lipid factor inside the hydrophobic pocket (Fig. 7B), VP0 helices on the sides of the 2-fold symmetry axis (Fig. 7E) and VP0 and VP3 alternating around a 3-fold (Fig. 7H). There is a molecule occupying the interprotomer pocket in CVB1-$VLP_{Tween80}$ not present in PDB ID 7DPF, as shown in Fig. 7A, D. Residues around the pocket do not differ from the native CVB1 (Fig. 7D). This pocket has been previously targeted as a potential antiviral target for other CVBs and was shown to have a role in the stability of the capsid[29,30].

Expanded CVB1-$VLPs_{Tween80}$ can be recognized by the lack of density below the 5-fold seen in Figs. 6C, G and I and 7A. There is no density corresponding to VP4 of VP0 in the expanded CVB1-$VLP_{Tween80}$ structure and no significant unmodeled density which would suggest a flexible region (Figs. 6C, G and I and 7A). Expansion at the 2-fold axis is consistent with expanded CVB1 A-particle (PDB ID 7DQ4) as seen in Fig. 7F, G and the lack of lipid factor and a collapsed hydrophobic pocket are in line with the A-particle structure (Fig. 7C)[5]. A notable difference is in the presence of the VP3 loop (aa170-188) which is lacking in 7DQ4 and the absence of the VP1 loop (aa 197–204) which is present in 7DQ4 (Fig. 7F, G). Both models start at residue 58 of VP1 (Fig. 7F, G). Residues on the VP3 loop are rotated away from the pore on the side of the 2-fold, potentially not blocking the VP1 N-terminus exit from the capsid (Fig. 7F)[5,8]. Unmodelled density shown at a threshold of 1.5 σ above mean on the sides of the 2-fold outside the capsid could be a flexible VP1 N-terminus (Supplementary Fig. 2B).

Compact $CVB1_{formalin}$ also exhibits structural characteristics of native CVB1, but due to the lower resolution at 4.1 Å, the level of detail is insufficient for a thorough comparison (Figs. 6J-R and 8A and B; Table 1). Differences compared to compact CVB1-$VLP_{Tween80}$ are the lack of the density for a lipid factor inside the pocket and density for the VP1 N-terminus on the inside of the capsid below VP4 (Fig. 8A). Another distinctive difference is the presence of the genome inside the capsid (Fig. 6O). Throughout the capsid, evidence of cross-linked residues could be observed, but were not modelled due to low resolution.

The expanded $CVB1_{formalin}$ at 3.01 Å-resolution allowed comparison at the atomic level to the expanded CVB1-$VLP_{Tween80}$ and CVB1 A-particles. Expanded $CVB1_{formalin}$ shares the same characteristics as the other structures including expansion as noticed by the pore at the 2-fold, lack of a lipid factor and collapse of the pocket. Whether the VP1 N-terminus is exiting the capsid is unclear due to heavy crosslinking of the capsid and

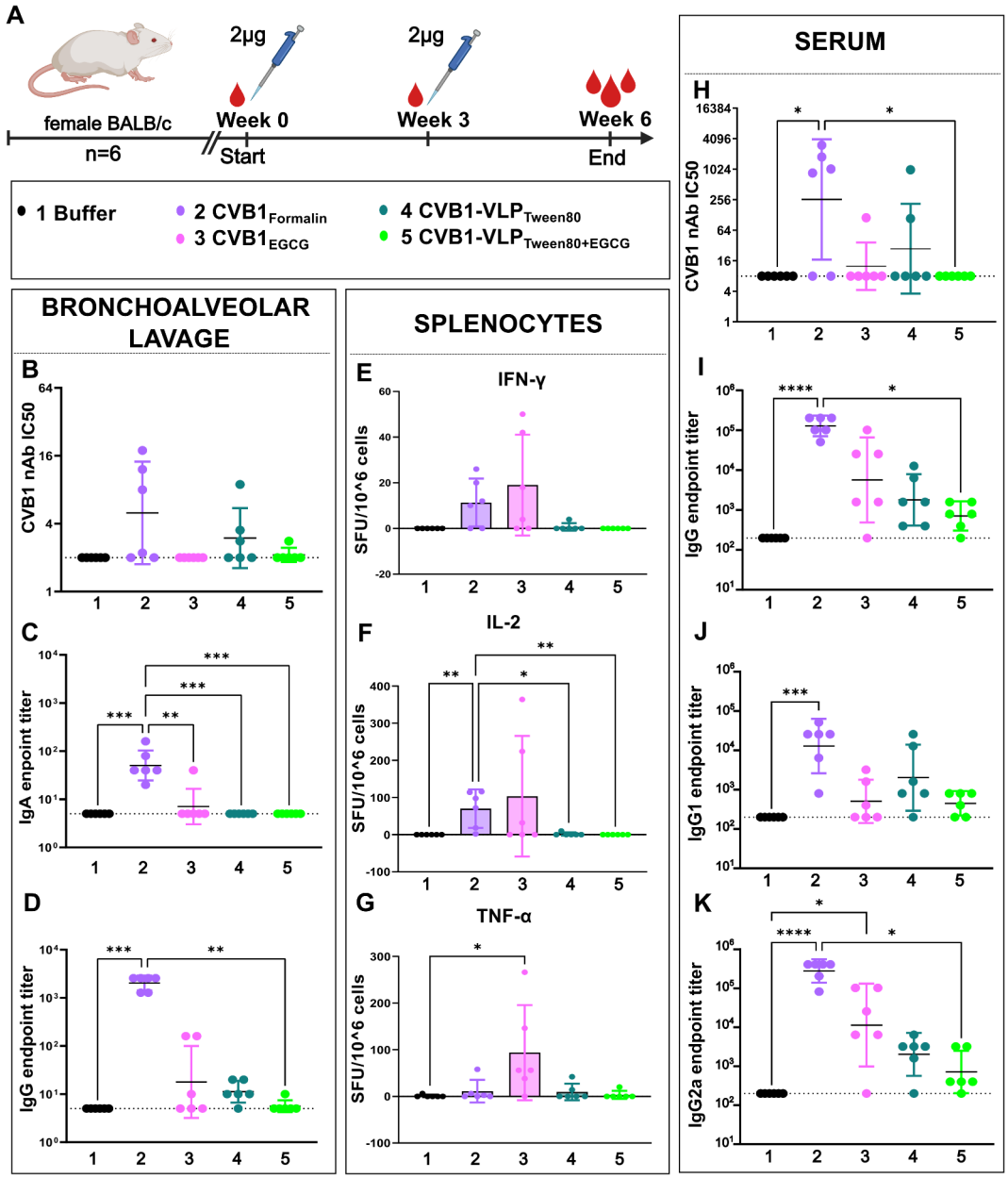

Fig. 5. Intranasal immunization. (**A**) Immunization schedule. (**B**) CVB1 neutralizing antibodies, (**C**) Vaccine antigen-specific IgA and (**D**) IgG antibody end point titers in bronchoalveolar lavage at week 6 after two intranasal immunizations. (**E**) IFN-γ, (**F**) IL-2 and (**G**) TNFα secreting splenocytes after stimulation with CVB1. (**H**) CVB1 neutralizing antibodies, (**I**) antigen-specific IgG, (**J**) IgG1 and (**K**) IgG2a antibodies from termination serum. Antigen specific antibodies were determined with indirect ELISA. Titers below 200 were assigned as negative. Neutralizing antibodies determined with microneutralization assay. Titers below 8 were assigned as negative. Shown as scatter dot plots with geometric mean and geometric SD. Cytokine secreting splenocytes were determined with FluoroSpot assay and shown as spot-forming units (SFU)/10^6 splenocytes, mean with SD. * = $p < 0.05$, ** = $p < 0.01$ *** = $p < 0.001$, **** = $p < 0.0001$.

several potential densities it could occupy (Fig. 8C-E). VP3 loop, similar to a CVB1-VLP$_{Tween80}$ structure, could occupy the quasi-3-fold pore and block the VP1 N-terminus, but the density for VP3 loop is weak compared to surrounding densities suggesting flexibility in the area. Furthermore, expanded CVB1$_{formalin}$ lacks density for VP4 and RNA (Figs. 6P and 8A). As observed in the compact CVB1$_{formalin}$ structure, heavy crosslinking is present throughout the capsid with residues contributing to most of the crosslinks being tryptophane, tyrosine and arginine and is occurring within and across different viral proteins (Fig. 8F). Similar to CVB1-VLP$_{Tween80}$ structures, a density which could house an ion at the 3-fold symmetry axis is observed in expanded CVB1$_{formalin}$ structure as well (Fig. 8F).

	compact CVB1-VLP$_{Tween80}$	expanded CVB1-VLP$_{Tween80}$	compact CVB1$_{formalin}$	expanded CVB1$_{formalin}$
Data collection and processing				
Magnification	105,000	105,000	150,000	150,000
Voltage (kV)	300	300	200	200
Electron exposure (e–/Å^2)	63.368	63.368	40	40
Defocus range (μm)	-0.2 to -1.6	-0.2 to -1.6	-0.1 to – 2.8	-0.1 to – 2.8
Pixel size (Å)	1.06	1.06	0.97	0.97
Symmetry imposed	I2	I2	I2	I2
Micrographs (no.)	13,860	13,860	615	615
Initial particle images (no.)	108,270	117,953	289	1935
Good particles	86,988	117,738	289	1935
Final particle images (no.)	86,988	117,738	289	1935
Map resolution (Å) FSC threshold	2.15 0.143	2.15 0.143	4.10 0.143	3.01 0.143
Map resolution range (Å)	999 – 1.94	999 – 1.94	999 – 1.94	999 – 1.94
Refinement				
Map sharpening *B* factor (Å^2)	-56.2	-65.1	-32.6	-100.7
Model composition Non-hydrogen atoms Protein residues				
VP1	56–278	58–197, 203–277	yes	58–197, 204–277
VP0 **VP2**	13–263	13–263	yes	12–43, 54–260
VP0 **VP4**	27–43	no	yes	no
VP3	1-238	1-232	yes	1-232
Ligands	Lipid, ?			
R.m.s. deviations				
Bond lengths (Å)	0.29	0.33	-	0.33
Bond angles (°)	0.48	0.50	-	0.50
Validation				
MolProbity score	1.55	2.27	-	2.27
Clashscore	3.36	5.84	-	5.84
Poor rotamers (%)	2.97	6.48	-	6.48
Ramachandran plot				
Favored (%)	97.78	95.12	-	95.12
Allowed (%)	2.22	4.29	-	4.29
Disallowed (%)	0	0.59	-	0.59

Table 1. Cryo-EM data collection, refinement and validation statistics.

Discussion

Adjuvants are generally categorized as immunostimulants and delivery systems and they are used to increase the immunogenicity of vaccines, especially in the case of protein-based vaccines. Certain adjuvants enhance immune activation by creating a depot for antigens at the injection site, prolonging antigen presence and attracting immune cells. This aids antigen absorption, induces local inflammation, and activates adaptive immune responses. Previous studies have demonstrated that EGCG prevents CVB1-infection[23], but the exact mechanism of action is not clear. One possible mechanism is nonspecific binding of EGCG to the CVB1 capsid.

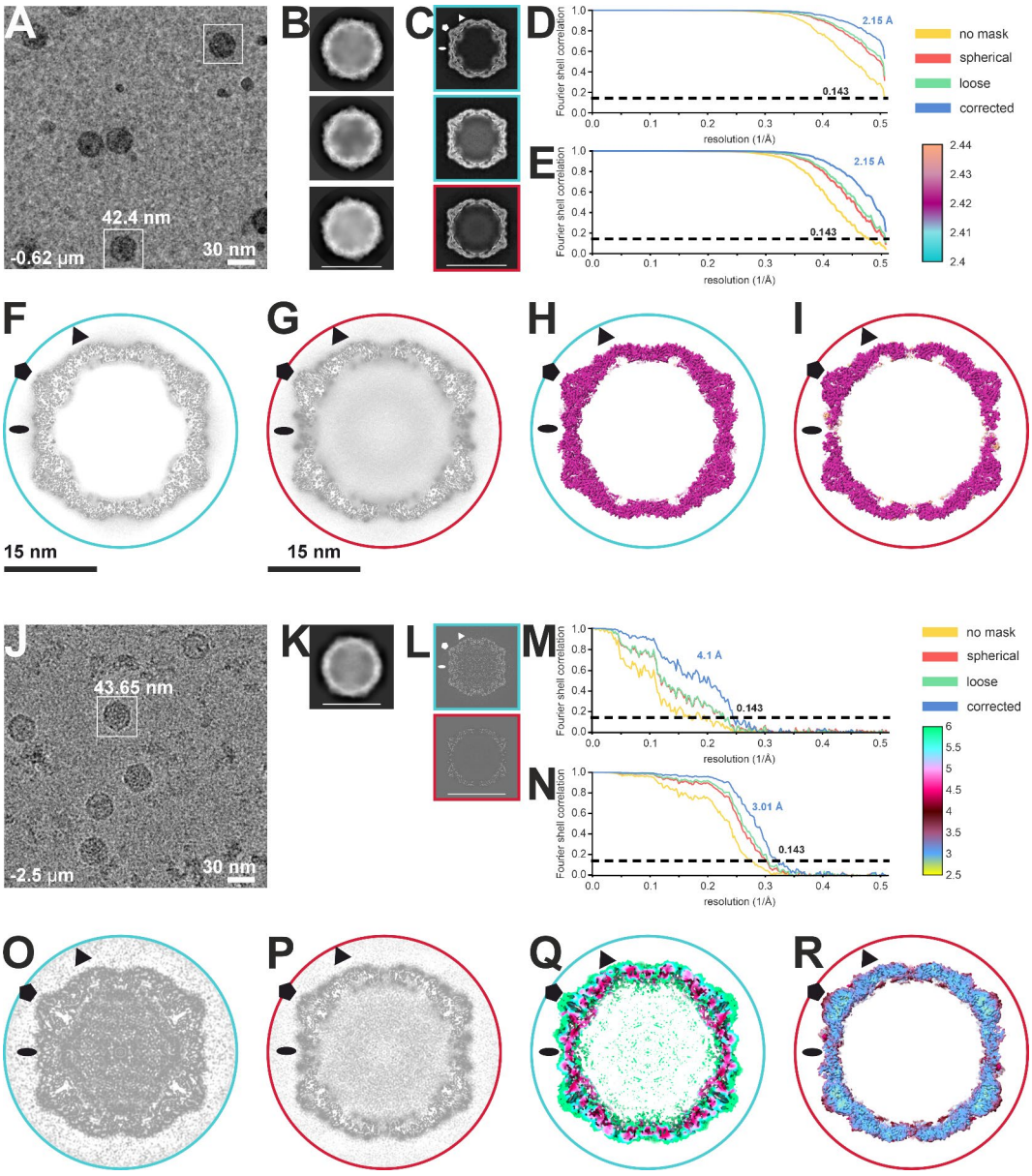

Fig. 6. CryoEM data collection and image processing. Panels A-I are related to CVB1-VLP$_{Tween80}$ dataset and J-R to CVB1$_{formalin}$ dataset. (**A**) and (**J**) Representative micrograph from each dataset. Scale bar is shown on the figure. An example of picked particles is boxed in white with a corresponding box size. (**B**) and (**K**) Representative 2D classes after final 2D classification of particles chosen for further processing obtained by Relion 4 in Scipion (**B**) or cryoSPARC (**K**). Scale bar of 30 nm is shown. (**C**) and (**L**) 3D classes obtained by Relion 4 in Scipion (**C**) or heterogeneous refinement in cryoSPARC (**L**). Particles in classes boxed in blue were chosen for further processing together within each dataset as they correspond to compact particles. Particles contributing to class boxed in red correspond to expanded particles. Symmetry axes are marked with elipse (2-fold), triangle (3-fold) and pentagon (5-fold). Scale bar of 30 nm is shown on the bottom figure. (**D**, **E**,**M**, **N**) Fourier shell correlation (FSC) curves for compact (**D**) and expanded (**E**) CVB1-VLP$_{Tween80}$ and compact (**M**) and expanded (**N**) CVB1$_{formalin}$ final reconstructions obtained by non-uniform refinement in cryoSPARC v4.2.0 (VLP) and v4.4.1 (formalin inactivated)[31]. The global resolution of CVB1-VLP$_{Tween80}$ structures is estimated at 2.15 Å as the estimation reaches the Nyquist limit. The legend for FSC curves calculated with different masks applied is on the right. (**F**, **G**,**O**, **P**) Central plane views of the final reconstructions for compact (**F**, **O**) in blue and expanded (**G**, **P**) in red. Symmetry axes are marked with elipse (2-fold), triangle (3-fold) and pentagon (5-fold). Scale bars of 15 nm are shown below the figures. (**H**, **I**, **Q**, **R**) Local resolution of final reconstructions for compact (**H**, **Q**) in blue and expanded (**I**, **R**) in red shown as a central slice of surface representation at 2.5σ above mean (**H**, **I**, **Q**) or 5.5 σ above mean (**R**). Local resolution values legend is shown in Ångstrom. Symmetry axes are marked with elipse (2-fold), triangle (3-fold) and pentagon (5-fold).

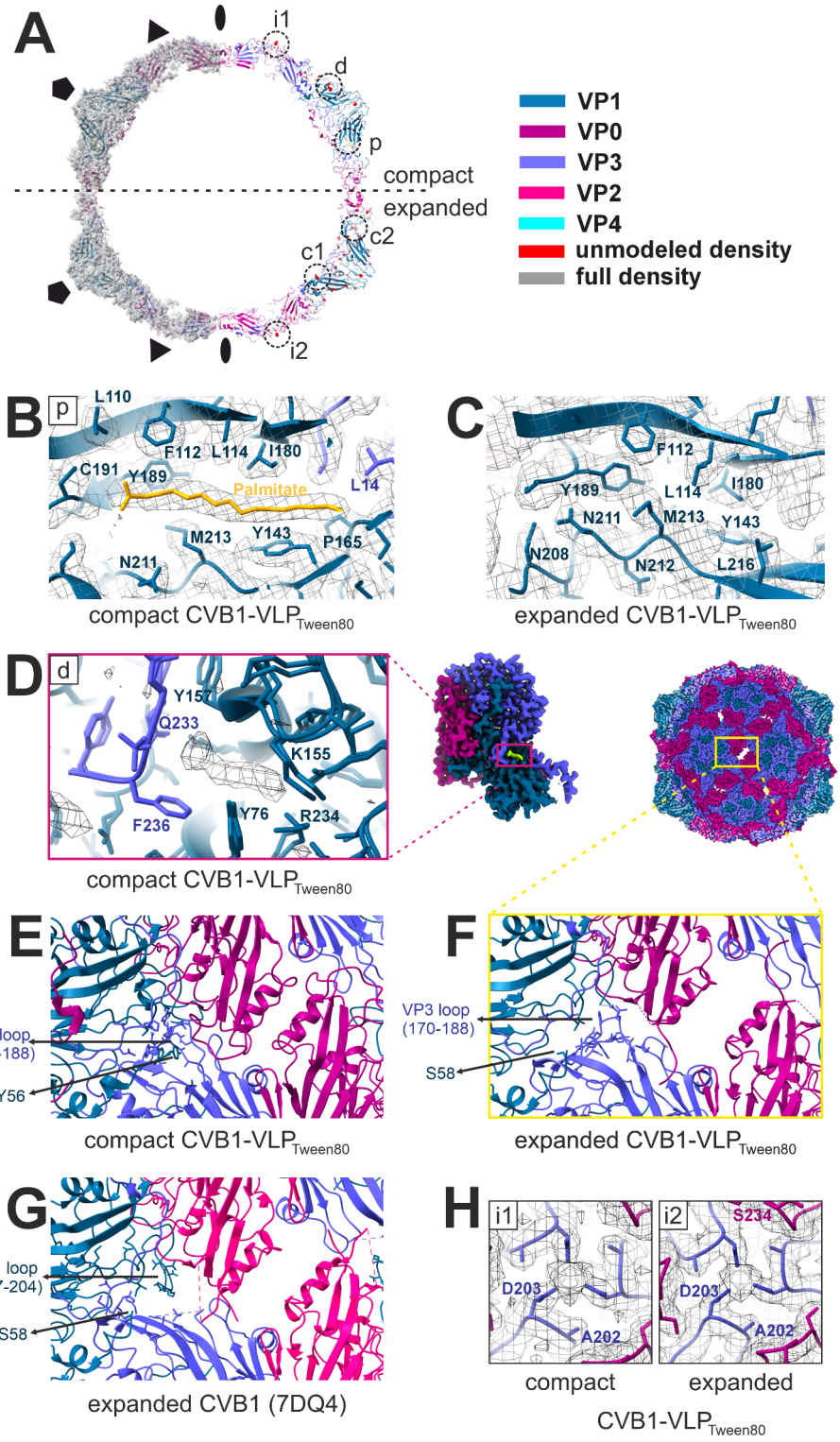

In this study, we investigated the binding capacity of EGCG to CVB1-VLP and CVB1 particles with DLS. Based on DLS-analysis, addition of EGCG to CVB1-VLP induced particle agglomeration, EGCG reversibly binding the capsids, forming over 1000 nm complex when EGCG was bound. Therefore, we hypothesized that the formed agglomerate may function as a storage unit in the immunization site, and we experimented with EGCG as a potential adjuvant for CVB1-VLP$_{No\text{-}Tween}$ via the subcutaneous immunization route. Our study compared the adjuvant effects of commercially used AS04 to the effects of EGCG. EGCG exhibited promising adjuvant properties for CVB1-VLP$_{No\text{-}Tween}$, as evidenced by higher levels of IgG1 and neutralizing antibodies (nAbs) compared to vaccines formulated with AS04 or without adjuvant (Fig. 3). This finding indicated the potential of EGCG as an effective adjuvant for enhancing vaccine-induced immune responses and warranted further investigation into its use.

◀**Fig. 7**. Final reconstruction analysis of compact and expanded CVB1-VLP$_{Tween80}$ obtained by cryoEM and single-particle reconstruction. (**A**) Final reconstructions shown as surface at 2.5σ above mean with fitted model (left) and the atomic model with unmodeled density in red (right). Unmodeled densities and positions of interest are marked with circles and are coded with small letters. (**B**) Focused view on the hydrophobic pocket (at position p on **A**) housing a lipid factor represented as palmitate in compact CVB1-VLP$_{Tween80}$. Density map is shown as mesh at 2.5σ above mean. (C) Focused view on the expanded CVB1-VLP$_{Tween80}$ density map on the site which corresponds to position in **B**). The pocket in the expanded particles is collapsed and there is no density corresponding to a lipid factor. Density map is shown as mesh at 2.5σ above mean. (**D**) Focused view on the interprotomer pocket (position d on **A**) of compact CVB1-VLP$_{Tween80}$ and native CVB1 (PDB ID 7DPF) located at the interface of two asymmetric subunits between VP1 and VP3 as shown on the right. Unmodeled density present in the interprotomer pocket of CVB1-VLP$_{Tween80}$ is shown as mesh at 2.5σ above mean on the left. On the right one asymmetric subunit is shown as surface at 2.5σ above mean with the unmodeled density in green. (**E**) – **G**) Focused views on the helices around the 2-fold symmetry axis and the VP3 loop of compact (**E**) and expanded (**F**) CVB1-VLP$_{Tween80}$ and expanded CVB1 (**G**) at position as shown in **F**). **H**) Focused view down the 3-fold symmetry axis. The density map is shown as mesh at 2.5σ above mean showing the unmodeled density between Ds of VP3 (positions i1 and i2 in **A**).

In poliovirus, formalin inactivation has been shown to cause destruction of some immunogenic epitopes compared to live vaccines, although it still allows cell attachment, the virus is less likely to undergo the conformational changes associated with entry and release of RNA[28]. Although formalin-inactivated vaccines continue to be important, VLPs are in contrast, highly amenable to sequence modifications, enabling the modification of epitopes and the incorporation of stabilizing mutations, thus enhancing their efficacy and versatility[9,10]. VLP vaccines have already been successfully generated for several enteroviruses[15,32–35].

Given the antiviral activity of EGCG against CVBs and other viruses[16–21,23,36], we evaluated the applicability of EGCG for inactivating CVB1, producing traditional inactivated whole-virus vaccine. We hypothesized that the absorption of antigens may be enhanced through mucosa when EGCG attaches to CVB1. We demonstrated that EGCG bound to CVB1 virus but required a much longer inactivation period than formalin inactivation. However, EGCG's antiviral activity might have been more rapid if the virus had been incubated with the compound at 37 °C, similar to the conditions used for formalin inactivation, as previously reported[23]. To our knowledge, this study is the first to explore the use of CVB1-VLP or formalin inactivated CVB1 as mucosal vaccines. While previous studies have successfully tested the intranasal immunization route for other enteroviruses, they employed adjuvants[37,38]. In contrast, we demonstrate that intranasal immunization with formalin-inactivated CVB1 alone can elicit strong and balanced immune responses even in the absence of adjuvants.

Mucosal immunization represents a promising strategy for inducing robust immune responses at the site of viral entry. EGCG has been shown to be a successful adjuvant when administered in combination with ovalbumin as a model antigen[39], showing increased mucosal IgA and systemic IgG, particularly IgG1[39]. Given our promising results on EGCG as a parenteral adjuvant, we investigated its efficacy in mucosal immunization using both CVB1-VLP$_{Tween80+EGCG}$ and CVB1 inactivated with EGCG (CVB1$_{EGCG}$). Contrary to our expectations, EGCG formulations combined with intranasal immunization did not enhance the mucosal immunity against CVB1 or CVB1-VLP$_{Tween80}$ in our preclinical model. Another study showed the co-administration of pro-vitamin A and EGCG with human immunodeficiency virus gp120 to have a synergistic effect enhancing the overall immune response. Interestingly and in line with our results, the intranasal administration of antigen administered only with EGCG without the pro-vitamin A, seemed to have a suppressive antigen-specific effect[40].

Although we were not able to enhance vaccine-specific immune responses with EGCG via mucosal route, the formalin-inactivated virus induced high antigen-specific humoral, cellular as well as mucosal immune responses. Notably, high antigen-specific IgG- and IgA-antibodies as well as neutralizing antibodies detected in the BAL of vaccinated mice indicates that formalin-inactivated CVB1 functions as a promising mucosal vaccine inducing robust and balanced immunity. Our hypothesis was that EGCG might stabilize certain CVB1 conformational epitopes and enhance processing of the antigens from the mucosa. However, our current findings challenge this hypothesis and indicate that the mucosal immune response is not enhanced by EGCG. Based on our findings, the immunogenic antibody-specific epitopes of CVB1 may have been damaged when EGCG bound to the virus. Interestingly, mice vaccinated with CVB1-VLP alone or formulated with EGCG intranasally induced weak antigen-specific IgG-, IgG1- and IgG2a-antibody responses in sera of vaccinated mice. This demonstrates that CVB1-VLP undergo antigen processing by immune cells when administrated via the mucosal route, but new mucosal adjuvants need to be developed or identified that induce more robust responses against VLPs.

We solved the atomic-resolution structure of CVB1-VLP$_{Tween80}$ and CVB1$_{formalin}$ that were used in the immunizations. Such knowledge was needed to be able to compare the particle structure and immunogenicity and to facilitate future modifications and optimizations producing more efficient VLP vaccines. Through cryoEM and single-particle image processing, two distinct particle populations were separated. These particle populations were termed compact and expanded, structurally corresponding to mature native CVB1 virions and CVB1 A-particles respectively[5]. Previously, it has been shown that both of these particle conformations can bind CVB1-specific neutralizing antibodies, demonstrating that at least the conformations of the analysed neutralizing-antibody epitopes were not affected by the viral allosteric process[41]. Here we observed two structural differences of CVB1-VLPs$_{Tween80}$ compared to native CVB1 which are the presence of a VP3 loop in the pore of the expanded CVB1-VLPs$_{Tween80}$ and an additional density in the interprotomer pocket of compact CVB1-VLP$_{Tween80}$. Both are unlikely to interfere with antibody binding and eliciting a lower immune response.

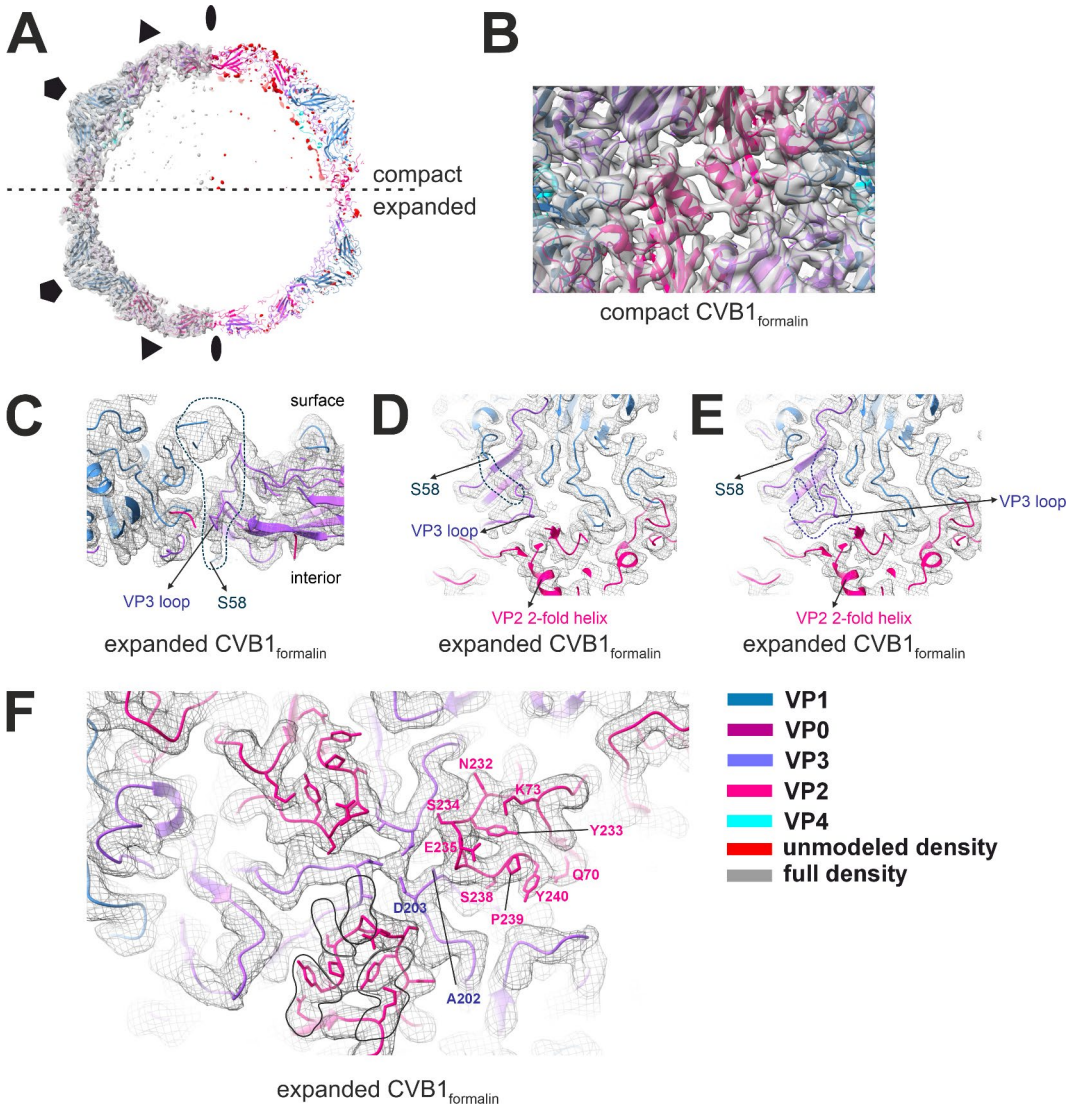

Fig. 8. Final reconstruction analysis of compact and expanded $CVB1_{formalin}$ obtained by cryoEM and single-particle reconstruction. (**A**) Final reconstructions shown as surface at 2.5 (compact) or 5.5 (expanded) σ above mean with fitted model (left) and the atomic model with unmodeled density in red (right). Symmetry axes are marked with elipse (2-fold), triangle (3-fold) and pentagon (5-fold). Color legend is in the bottom right corner of the figure. (**B**) Focused view along the 2-fold axis of compact $CVB1_{formalin}$ shown as model fitted into density map represented as surface at 2.5σ above mean. C-F. Focused view on the expanded $CVB1_{formalin}$ shown as model fitted into density map represented as mesh at 5.5σ above mean. (**C**) View through a slice of the capsid showing the beginning of VP1 N-terminus (S58) and VP3 loop at the quasi-3-fold pore. Density for possible VP1 N-terminus is marked with a dotted line and is clashing with VP3 loop. (**D**) and (**E**) View of the quasi-3-fold pore with potential alternative densities which could be modelled marked with a dotted line for VP1 N-terminus (**D**) or VP3 loop (**E**). (**F**) View on the surface of the capsid at the 3-fold symmetry axis. Density for ion is visible at the center of the 3-fold coordinated by 3 Asp. Cross-linking due to formalin treatment is circled in black on one asymmetric subunit. Residues of interest are marked on another asymmetric subunit. Cross-linking occurs both within and across different viral proteins.

We demonstrated that the distribution of the particle populations is 85–15% in favour of the expanded particles in formalin-inactivated virus, whereas the ratio was 48% compact to 52% expanded for VLPs, demonstrating a marked difference in the proportions between the vaccines. In contrast to earlier studies with poliovirus where formalin inactivation prevent expansion[28], in our preparation, expansion and loss of genomic RNA occurred, yet immunogenicity was still good. This agrees with work by Zheng et al. on CVB1 nAb[41] which showed the ability of three neutralizing antibodies to bind to all conformations of CVB1, including empty particles and A-particles, and compete with the receptor for binding while inducing high immune response[41]. The same observation was made with Enterovirus A71 VLPs[42]. Interestingly, nAb 8A10 studied in[41] has an epitope at the same site where the additional density was observed in the interprotomer pocket of compact CVB1-$VLP_{Tween80}$. Therefore, it is unlikely that the additional density would block antibody binding due its small size but alludes

to the importance of VLP expression system and purification conditions. However, here two potential reasons for the lower CVB1-$VLP_{Tween80}$ immunogenicity compared to formalin inactivated virus are the lack of RNA in the VLP, and epitope conformation preservation by formalin. Differences of $CVB1_{formalin}$ and native CVB1 include heavily cross-linked capsid and potential internalisation of VP1 N-terminus in expanded $CVB1_{formalin}$. Internalized N-terminus would not be accessible to antibodies and may elicit a different response than that of expanded CVB1-$VLPs_{Tween80}$. Furthermore, none of the cross-linked sites coincide with antibody epitopes discussed in Zhen et al.[70] Which form of the particles is responsible for the immune response is not known, but the presence of a large population of expanded particles does not seem to hinder the vaccine potential of formalin inactivated virus. Despite the lower immunizing properties, VLPs were stable for at least one month and can handle freezing and thawing while retaining almost 50% of the particles in the compact form.

Structural and immunogenicity results from this study indicate that the lower neutralizing antibody responses for CVB1-VLP vaccine candidates via the mucosal route compared to formalin-inactivated CVB1 may be due to the presence of RNA in the inactivated virus vaccine, as RNA is absent from the VLP vaccine. It has been shown widely previously that the presence of RNA in the vaccine functions as adjuvant, enhancing the overall immune response by activating innate immune pathways by activation of pattern recognition receptors and subsequent activation of adaptive immunity[43]. Further studies, such as affinity maturation assessments could help clarify the difference further. In conclusion, our results highlight the potential of using formalin inactivated CVB1 vaccine in mucosal immunization programs. However, as traditional manufacturing cannot be applied to several enteroviruses (or other viruses), our results highlight the importance of further development for next-generation VLP-based vaccines. The atomic resolution structural data presented here for CVB1-VLP enables further developments for the candidate vaccine holding a promise for developing vaccine platform that can be applied for all enteroviruses.

Materials and methods

Coxsackie B1 Virus-Like particle (CVB1-VLP) and virus production and purification

A wild CVB1 field isolate (CVB1-10796, isolated from Argentina 1983[44], kindly provided by Centers for Disease Control and Prevention, Division of Viral Diseases), gene bank accession number PP782006, was used in producing the formalin inactivated CVB1 vaccine and as a template for CVB1-VLP. To produce CVB1-VLPs, a baculoviral transfer vector pOET5, which included distinct cassettes for the CVB1 VP0-3 polyprotein regulated by the polyhedrin promoter and the 3CD-protease controlled by the CMV promoter, was ordered from GenScript. The recombinant baculovirus was generated following the guidelines outlined in the FlashBAC baculovirus expression system (Oxford Expression Technologies) manual and utilizing the flashBAC ULTRA baculovirus genome. CVB1-VLPs were produced in High-Five insect cells with a multiplicity of infection (MOI) value of 1. Two separate purifications were performed for CVB1-VLPs using previously established purification method[14]. The VLPs were purified and stored without and with Tween80 (designated $VLP_{No-Tween80}$ and $VLP_{Tween80}$). Briefly, after harvesting the culture supernatant containing the VLPs, it was clarified by centrifugation (9610×g, 4 °C, 30 min) and was filtered through a 0.2 µm filter. The VLPs were concentrated from the culture supernatant by Tangential Flow Filtration (TFF), utilizing 750 MWCO hollow fiber with an ÄKTA Flux system (Cytiva). The buffer was exchanged to 40 mM Tris pH 7.5, 10 mM $MgCl_2$, 40 mM NaCl, with the same system. Impurities were removed from the preparation using HiTrap Q and SP columns (GE Healthcare), as well as CIMmultus QA and SO_3 ion exchange chromatography (IEX) columns (BIASeparations). For $VLP_{No-Tween80}$ additional baculovirus removal step was included utilizing POROS CaptureSelect BacuClear Affinity Matrix (Thermo Fischer Scientific). Endotoxins were removed with EndoTrap® HD FPLC column (LIONEX), in accordance with the relevant guidelines and regulations. CVB1-$VLP_{No-Tween80}$ and CVB1-$VLP_{Tween80}$ were stored in Tris-buffered saline (40 mM Tris-HCl pH 7.4, 10 mM $MgCl_2$, 0.2 M NaCl) without or with 0.1% Tween80 at -80 °C.

CVB1 virus was produced in Green Monkey Kidney (GMK) cells that were kindly provided by the Finnish Institute for Health and Welfare (Virology Department). GMK cells were cultivated in MEM with Earle's salts, 2 mM L-glutamine and sodium bicarbonate supplemented with 10% FBS and 1% penicillin-streptomycin (all from Sigma-Aldrich). The virus was propagated in GMK cells in multilayer (Falcon Cell culture Multi-Flask or Corning hyperflask M cell culture vessel) flasks using SFM4MegaVir protein-free medium (HyClone) without FBS for 2–5 days with MOI value of 5–10. Purification of the virus was performed similarly as previously[11]. Briefly, the viruses were recovered from the clarified GMK cell culture supernatant by 30% sucrose cushion pelleting (175,000 x g, 16 h at 4 °C). The pellets were resuspended in phosphate-buffered saline (PBS)–0.1% Tween80 and were inactivated in 0.01% (v/v) formalin for 5 days at 37 °C or with 524 µM EGCG for 28 days in RT. Virus inactivation was confirmed by the lack of infectious virus (after culturing the inactivated viruses in GMK cells) in $TCID_{50}$ (median tissue culture infectious dose) end-point dilution assay (detection limit, 49 $TCID_{50}$ units/ml). Briefly, first, a 6-fold CVB1 dilution series with eight replicates was made in 96-well plate. Viruses were diluted to Hanks balanced salt solution (HBSS) with 0.01 M HEPES and 0.6% FBS (all from Sigma-Aldrich). 16 000 GMK cells in Minimum Essential Medium Eagle (MEM, Sigma-Aldrich) containing 5% FBS, were seeded on top of the virus dilutions. Viruses were allowed to infect cells for 46 h in a humidified incubator at + 37 °C with 5% CO_2. 10 µl of AlmarBlue Cell Viability Reagent (Invitrogen) was then added to the wells and the cells were incubated 2 h in 37 degrees at CO_2 incubator. Then, the fluorescence was measured with 560 nm excitation and 590 nm emission wavelengths using Envision UV/VIS (Perkin Elmer) multiplate reader. The fluorescent signal generated from the assay is proportional to the number of living cells in the sample. $TCID_{50}$ calculation was based on Karber's formula[45].

CVB1-VLP and virus characterization

Purified VLPs and viruses were analyzed with mini-protean TGX stain-free precast gels (Bio-Rad). Virus and VLP proteins and impurities were assessed by densitometry analysis of SDS-PAGE gels using the ImageJ

Fiji software v2.16.0[46], https://imagej.net/. VP1 and VP3 proteins were detected by Western blotting using a rabbit anti-CVB1-6 polyclonal antibody[11]. A mouse monoclonal anti-gp64 antibody (1:2000, Santa Cruz Biotechnology) was used to identify residual baculovirus in the purified CVB1-VLPs. IRDye 680RD goat anti-rabbit and IRDye 800CW goat anti-mouse secondary antibodies (1:20 000, LI-COR Biosciences) were used for visualization. Determination of VLP and inactivated virus total protein concentration, dynamic light scattering (DLS) analysis and transmission electron microscopy (TEM) imaging were performed as described[15].

Cryo-Electron microscopy structural determination of CVB1-VLP and formalin inactivated CVB1

Purified CVB1-$VLP_{Tween80}$ stored at -80 °C in Tris-buffered saline (40 mM Tris-HCl + 10 mM $MgCl_2$ + 0.2 M NaCl + 0.1% Tween80, pH 7.3) at a concentration of 2 mg/ml and purified CVB1 virus treated by formalin (as described in Sect. 1) and stored at -80 °C were applied to glow-discharged Quantifoil R1.2/1.3 300 mesh copper grids with 2 nm carbon film. A 3 µl aliquot was incubated on the grid for 15 s and blotted for 1.5 s before vitrification in liquid ethane using a semi-automatic plunger Leica EM GP. The chamber was set to 85% humidity, 22 °C.

CVB1-$VLP_{Tween80}$ data was collected at SciLifeLab in Sweden using a Titan Krios equipped with Gatan K3 detector and operating at 300 kV. 40 frames per image were collected at 105 000 * nominal magnification resulting in 1.06 Å/pixel with a total dose of 63.368 $e^-/Å^2$. Images were taken between − 0.4 and − 1.6 µm from focus at 0.2 µm defocus increments. Data collection details and statistics are described in Table 1; Fig. 6. $CVB1_{formalin}$ data was collected at CryoEM unit at the University of Helsinki using a FEI Talos Arctica equipped with a Falcon III detector and operating at 200 kV. 40 frames per image were collected at 150 000 * nominal magnification resulting in 0.97 Å/pixel with a total dose of 40 $e^-/Å^2$. Images were taken between − 0.1 and − 2.8 µm defocus. Data collection details and statistics are described in Table 1; Fig. 6.

Images were processed in cryoSPARC v4.2.0, v4.4.1[31], https://cryosparc.com/ and Scipion v3.0.12[47], https://scipion.i2pc.es/. Movies were motion and ctf corrected using Patch Motion Correction and Patch CTF Estimation from cryoSPARC[31]. A small set of particles was picked using Manual Picker in cryoSPARC and classified reference-free in 2D[31]. A representative class was used to generate a template for Template Picker in cryoSPARC[31]. A box size of 400 pixels was used to extract picked particles from the CVB1-$VLP_{Tween80}$ dataset and 450 pixels box size for particles from $CVB1_{formalin}$ dataset. Particles were iteratively classified in 2D after which classes containing particles were selected for further processing. Further processing differs for CVB1-$VLP_{Tween80}$ and $CVB1_{formalin}$ datasets. For the CVB1-$VLP_{Tween80}$ dataset, a subset of randomly chosen 10 000 particles was used to generate 3 ab initio models[31]. The model with the highest number of different views created from 3 866 particles was used for homogeneous refinement in cryoSPARC using the full particle set[31]. Particles were exported to Scipion v3.0.12[47] and classified in 2D and 3D using Relion 4[47–52], https://relion.readthedocs.io/en/release-4.0/. Classification using Relion allowed for separation of compact and expanded particles. Particles were imported back to cryoSPARC in separate sets and locally CTF refined[50]. Non-uniform refinement was applied to improve the resolution. Parameters for non-uniform refinement were changed to correct for the curvature of the Ewald Sphere, optimize per-particle defocus and per-group CTF parameters[53]. For $CVB1_{formalin}$ initial models used were final reconstructions of expanded and compact CVB1-$VLPs_{Tween80}$ filtered to 30 Å. The models were used as input to heterogeneous refinement in cryoSPARC resulting in the separation of particle populations corresponding to native CVB1 and CVB1 A-particles[5]. Particles were further CTF refined locally and underwent non-uniform refinement with correction for the curvature of the Ewald Sphere, optimized per-particle defocus and per-group CTF parameters[53]. Details of the image processing and refinement statistics for each data can be found in Table 1. The local resolution was estimated by utilizing the local resolution estimation tool in cryoSPARC[31]. The resolution of the final reconstructions was estimated according to the gold standard Fourier Shell Correlation of 0.143 threshold criterion and local resolution using Local Resolution job in cryoSPARC[31,54].

Modeling

The CVB1 atomic models PDB ID 7DPF and 7DQ4 were rigidly fitted into the compact and expanded CVB1-$VLP_{Tween80}$ reconstructions, respectively, in UCSF ChimeraX v1.5[5,55,56], https://www.cgl.ucsf.edu/chimerax/. The backbone was fitted using 3D refinement in Phenix v1.20.1, https://phenix-online.org/ and the sidechains were manually adjusted in Coot 0.9.8.1[57,58], https://www2.mrc-lmb.cam.ac.uk/personal/pemsley/coot/. Additional residues could be added based on the sequence of CVB1-$VLP_{Tween80}$. Residues which had no corresponding density were deleted. The final models were validated using the MolProbity server and cryoEM validation in Phenix v1.20.1[58,59]. To obtain the difference map between modeled and unmodeled density, maps were created in UCSF ChimeraX v1.5 from the symmetrized models at 2.4 Å resolution and subtracted using the subtract tool[55,56]. Table 1 shows the details of modeling and validation. The resolution of compact $CVB1_{formalin}$ was insufficient for atomic modelling. Expanded CVB1-$VLP_{Tween80}$ model was used as the basis for modeling expanded $CVB1_{formalin}$ structure using the same protocol. All the structure related figures were made in ChimeraX[40,41] and CorelDraw2023, https://www.coreldraw.com/en/.

Vaccine preparation, immunizations and sampling of mice

In the pilot study, CVB1-$VLP_{No-Tween80}$ was used to evaluate the immune responses to VLP with different compounds. We wanted to analyze the immunogenicity of the VLP alone, VLP together with an adjuvant that is used in commercial protein-based vaccines (AS04) and $VLP_{No-Tween80}$ with a potential new adjuvant EGCG. Vaccines were diluted to 2 µg per 150 µl dose using Tris buffer (20mM Tris-HCl pH 7.4 + 5 mM $MgCl_2$ + 20mM NaCl) as a diluent. A mixture of AS04 components; 5 µg MPLA-SM VaccineGrade (Invivogen) dissolved in DMSO and 50 µg of 2% Alhydrogel (Invivogen) per dose was added prior to administration and left to bind in constant mixing for 10 min at room temperature. 6 µg of EGCG (purchased from Sigma-Aldrich and dissolved

in distilled water in stock concentration 3 mg/mL) per dose was left to bind for 1 h at room temperature prior to immunization. 6-week-old female BALB/cJRj mice (Janvier Labs) were randomly divided into groups of 3 mice and were given a 150 µl dose subcutaneously (s.c.) on week 0 and 3. Mice were euthanized on week 6 and blood samples were collected to Microtainer SST Blood Collection Tubes (Becton Dickinson).

To study the mucosal immune responses for inactivated CVB1 virus and CVB1-VLP$_{Tween80}$, vaccines were diluted to 2 µg in 25 µl per dose using PBS (pH 7.4) as a diluent. Inactivation of CVB1 was performed with formalin like described[11] or with EGCG. For the CVB1-VLP$_{Tween80+EGCG}$ group, 6 µg of EGCG was added to the preparation and incubated 2 h at room temperature prior to vaccinations. 9-week-old female BALB/cJRj (Janvier Labs) were used. Six animals were randomly assigned per group and 2 µg of vaccine antigen was administered intranasally (i.n.) by pipetting a volume of 12.5 µl to each nasal opening (total volume of 25 µl). To evaluate the mucosal immune responses, bronchoalveolar lavages were collected upon termination as described[60], using PBS with Pierce Protease Inhibitor tablets (Thermo Fisher Scientific) and centrifuged 20 000 x g, + 4 °C, 5 min before storing at -20 °C until further use in enzyme-linked immunosorbent assays (ELISA).

All efforts were made to minimize animal suffering and reduce the number of animals used in this study. Administration volumes 150 µl s.c. and 25 µl i.n. were based on the recommendations by the Finnish Regional State Administrative Agency and Diehl et al. 2001[61]. Procedures were conducted under 2–4% isoflurane (Attane Vet, Vet Medic Animal Health) inhalation to minimize stress. Animals in the pilot study were euthanized in a CO_2 chamber, followed by whole blood collection via cardiac puncture. Mice in the mucosal immunization study were euthanized by exsanguination through axillary vein puncture, under anesthesia induced by a lethal dose of ketamine hydrochloride (Ketaminol Vet, MSD Animal Health) and medetomidine hydrochloride (Dorbene Vet, Vetcare Oy), ensuring successful BAL sampling.

Upon arrival, animals were let to acclimatize for a week before any experiments were started. All mice were housed in a pathogen-free environment in individually ventilated cages and food and water was provided *ad libitum*. The welfare of the animals was monitored daily throughout the experiment. All experiments in this study were carried out following the Finnish Act on the Protection of Animals Used for Scientific or Educational Purposes (497/2013). Procedures were approved by the Regional State Administrative Agency, Pirkanmaa, Finland (decision number ESAVI/1408/2021). All animal reporting was conducted in accordance with ARRIVE guidelines.

Antigen specific IgG, IgG subtype and IgA antibodies post vaccination

To evaluate the immune response elicited by the vaccination, total antigen-specific IgG antibodies, and two IgG subtypes were determined. IgG1 as an indicator of the humoral (Th2-type) immune response and IgG2a subtype as an indicator of the cellular (Th1-type) immune response. The IgG1 to IgG2a ratio was also calculated as an average for each group. IgG1:IgG2a ratios ≤ 0.5 indicate a Th1-biased immune response, while a ratio of ≥ 2.0 indicates a Th2-biased immune response. Ratios between 0.5 and 2.0 indicate a mixed response[27].

Antigen-specific IgG, IgG1, IgG2a and IgA antibodies were determined with indirect ELISA as previously described[15]. 50 ng of CVB1-VLP$_{Tween80}$ per well was used as the coating antigen across all study groups. HRP conjugated anti-mouse secondary antibodies IgG (1:3000), IgG1 (1:1000) and IgG2a (1:1000) from Invitrogen were used to detect antigen specific IgG and IgG subtype antibodies in the serum. In addition, HRP-conjugated goat anti-mouse IgA (1:1000, Invitrogen) was used to detect IgA antibodies in bronchoalveolar lavage (BAL). Positivity cut-off value for the end-point titer was determined with buffer control mice OD values with average OD + 3*SD.

The final antibody dilution above the experimental cutoff value was determined as the end-point titer for the antibody. End-point titer values for each sample were plotted in graphs expressing the geometric mean titer (GMT) of each experimental group. GMT calculation was performed by taking the antilog of the mean of the log titer transformation. The positivity cutoff value was given an arbitrary value of half of the titer of which the 2-fold serum or BAL dilutions were started (positivity cutoff being 1:200 dilution for serum and 1:5 for BAL).

Neutralizing antibodies

To analyze the CVB1 neutralizing capacity of the vaccinated mice sera and BAL samples, neutralizing antibodies against a live virus were measured by cell viability based micro-neutralization assay using GMK cells. First, two-fold serial dilution series of serum and BAL were prepared in duplicate in HBSS with 0.01 M HEPES and 0.6% FBS (all from Sigma-Aldrich) into a 96-well plate. 50 x $TCID_{50}$ units of the CVB1 virus was added per well and incubated at 37˚C for 1 h to allow neutralizing antibodies to bind the viruses. Then, 16 000 GMK cells in Minimum Essential Medium Eagle (Sigma-Aldrich) containing 5% FBS, were seeded on top of the pre-incubated virus and serum dilutions. After 46 h of incubation in a humidified incubator at + 37 °C with 5% CO_2, 10 µl of AlamarBlue Cell Viability Reagent (Invitrogen) was added to the wells and the fluorescent signal generated from the assay was measured like described for $TCID_{50}$ assay. Neutralization curves were plotted in GraphPad Prism 9.0.0 Software using 4-PL curve fitting constrained to 0% at the bottom and to 100% at the top and the inhibitory concentration value was determined from each curve. The 50% neutralizing titer designated as inhibitory concentration (IC_{50}) in Prism 9.0.0 was defined by the midpoint of the sample-specific neutralization curve. The geometric means of the IC_{50}-titers (with geometric standard deviation) were plotted on the graphs presenting the neutralizing antibody responses.

T-cell specific cytokine secretion from stimulated splenocytes

Mouse FluoroSpot^{PLUS} assay kit (Mabtech) was used to measure the levels of IFN-γ, IL-2, and TNF-α secreted from lymphocytes extracted from spleens of the vaccinated mice. Upon termination, the spleens were collected and splenocytes were extracted as follows: organs were minced through sterile 40 µm cell strainers (Thermo Fisher Scientific) and washed with PBS + 1% FBS + 2 mM EDTA. Cells were centrifuged and red blood cells were

lysed with 1 ml of ACK buffer (Gibco) for 1 min. Lysed cells were removed by washing with PBS + 1% FBS + 2 mM EDTA. Cells were seeded in duplicates with the concentration of 2.5×10^5/well in RPMI1640 GlutaMAX Medium (Thermo Fisher Scientific), supplemented with 25 mM HEPES and penicillin-Streptomycin (1:100) and 10% FBS (all from Sigma-Aldrich). Splenocytes were stimulated in vitro with CVB1 (1 µg/well, for 18 h in an incubator at 37 °C, 5% CO_2). Concanavalin A (Sigma-Aldrich) (2 µg/well) and culture medium were used as positive and negative controls. The following experimental procedures were carried out in accordance with the relevant guidelines and regulations. The spot-forming cells were counted with Mabtech IRIS ELISpot/FluoroSpot reader (service by MabTech, Stockholm, Sweden). The positivity cut-off value for each mouse was determined individually as the average count of spots in the negative control wells + 3*SD. The resulting frequencies of responsive cells were reported as the number of spot-forming units per 10^6 splenocytes.

Statistical analyses

Statistical analyses were done with GraphPad Prism 9.0.0 for Windows, GraphPad Software, www.graphpad.com. Immunological data was treated as non-parametric and the comparison between multiple groups was done using Kruskal Wallis t-test followed with Dunn's Multiple Comparison test.

Data availability

The datasets used and/or analyzed during this study are available from the corresponding author on reasonable request. The atomic models and cryoEM densities are deposited in the wwPDB with accession numbers PDB:9FJC and EMD-50497 for compact CVB1-$VLP_{Tween80}$, PDB:9FJD and EMD-50498 for expanded CVB1-$VLP_{Tween80}$, PDB:9FJE and EMD-50500 for expanded $CVB1_{formalin}$, EMD-50499 for compact $CVB1_{formalin}$. The sequence for the CVB1-10796 can be accessed in GenBank with accession number PP782006.

Received: 5 December 2024; Accepted: 17 March 2025
Published online: 25 March 2025

References

1. Wong, A. H., Lau, C. S., Cheng, P. K., Ng, A. Y. & Lim, W. W. Coxsackievirus B3-associated aseptic meningitis: an emerging infection in Hong Kong. *J. Med. Virol.* **83**, 483–489 (2011).
2. Huber, S. & Ramsingh, A. I. Coxsackievirus-induced pancreatitis. *Viral Immunol.* **17**, 358–369 (2004).
3. Kim, K. S., Hufnagel, G., Chapman, N. M. & Tracy, S. The group B coxsackieviruses and myocarditis. *Rev. Med. Virol.* **11**, 355–368 (2001).
4. Rossmann, M. G. et al. Structure of a human common cold virus and functional relationship to other picornaviruses. *Nature* **317**, 145–153 (1985).
5. Xu, L. et al. Cryo-EM structures reveal the molecular basis of receptor-initiated coxsackievirus uncoating. *Cell. Host Microbe.* **29**, 448–462e5 (2021).
6. Richardson, J. S. The anatomy and taxonomy of protein structure. in Advances in Protein Chemistry (eds Anfinsen, C. B., Edsall, J. T. & Richards, F. M.) vol. 34 167–339 (Academic, (1981).
7. Basavappa, R. et al. Role and mechanism of the maturation cleavage of VP0 in poliovirus assembly: structure of the empty capsid assembly intermediate at 2.9 A resolution. *Protein Sci.* **3**, 1651–1669 (1994).
8. Domanska, A. et al. Structural studies reveal that endosomal cations promote formation of infectious coxsackievirus A9 A-Particles, facilitating RNA and VP4 release. *J. Virol.* **96**, e0136722 (2022).
9. Ding, X., Liu, D., Booth, G., Gao, W. & Lu, Y. Virus-Like particle engineering: from rational design to versatile applications. *Biotechnol. J.* **13**, e1700324 (2018).
10. Lua, L. H. et al. Bioengineering virus-like particles as vaccines. *Biotechnol. Bioeng.* **111**, 425–440 (2014).
11. Hankaniemi, M. M. et al. Optimized production and purification of coxsackievirus B1 vaccine and its preclinical evaluation in a mouse model. *Vaccine* **35**, 3718–3725 (2017).
12. Stone, V. M. et al. A hexavalent coxsackievirus B vaccine is highly Immunogenic and has a strong protective capacity in mice and nonhuman primates. *Sci. Adv.* **6**, eaaz2433 (2020).
13. Hankaniemi, M. M. et al. A comparative study of the effect of UV and formalin inactivation on the stability and immunogenicity of a coxsackievirus B1 vaccine. *Vaccine* **37**, 5962–5971 (2019).
14. Hankaniemi, M. M. et al. Formalin treatment increases the stability and immunogenicity of coxsackievirus B1 VLP vaccine. *Antiviral Res.* **171**, 104595 (2019).
15. Hankaniemi, M. M. et al. Structural insight into CVB3-VLP Non-Adjuvanted vaccine. *Microorganisms* **8** https://doi.org/10.3390/microorganisms8091287 (2020).
16. Ciesek, S. et al. The green tea polyphenol, epigallocatechin-3-gallate, inhibits hepatitis C virus entry. *Hepatology* **54**, 1947–1955 (2011).
17. Calland, N. et al. -)-Epigallocatechin-3-gallate is a new inhibitor of hepatitis C virus entry. *Hepatology* **55**, 720–729 (2012).
18. He, W., Li, L. X., Liao, Q. J., Liu, C. L. & Chen, X. L. Epigallocatechin gallate inhibits HBV DNA synthesis in a viral replication - inducible cell line. *World J. Gastroenterol.* **17**, 1507–1514 (2011).
19. Imanishi, N. et al. Additional inhibitory effect of tea extract on the growth of influenza A and B viruses in MDCK cells. *Microbiol. Immunol.* **46**, 491–494 (2002).
20. Yamada, H., Takuma, N., Daimon, T. & Hara, Y. Gargling with tea Catechin extracts for the prevention of influenza infection in elderly nursing home residents: a prospective clinical study. *J. Altern. Complement. Med.* **12**, 669–672 (2006).
21. Ho, H. Y., Cheng, M. L., Weng, S. F., Leu, Y. L. & Chiu, D. T.-Y. Antiviral effect of Epigallocatechin gallate on enterovirus 71. *J. Agric. Food Chem.* **57**, 6140–6147 (2009).
22. Cheong, Y. et al. Epigallocatechin-3-Gallate as a novel vaccine adjuvant. *Front. Immunol.* **12**, (2021).
23. Reshamwala, D. et al. Polyphenols Epigallocatechin gallate and Resveratrol, and Polyphenol-Functionalized nanoparticles prevent enterovirus infection through clustering and stabilization of the viruses. *Pharm. 2021.* **13**, 1182 (2021).
24. Kundi, M. New hepatitis B vaccine formulated with an improved adjuvant system. *Expert Rev. Vaccines.* **6**, 133–140 (2007).
25. Stone, V. M. et al. A coxsackievirus B vaccine protects against virus-induced diabetes in an experimental mouse model of type 1 diabetes. *Diabetologia* **61**, 476–481 (2018).
26. Stone, V. M. et al. Coxsackievirus B Vaccines Prevent Infection-Accelerated Diabetes in NOD Mice and Have No Disease-Inducing Effect. *Diabetes* db210193 (2021). https://doi.org/10.2337/db21-0193
27. Yang, K. et al. A DNA vaccine prime followed by a Liposome-Encapsulated protein boost confers enhanced mucosal immune responses and Protection1. *J. Immunol.* **180**, 6159–6167 (2008).

28. Wilton, T., Dunn, G., Eastwood, D., Minor, P. D. & Martin, J. Effect of formaldehyde inactivation on poliovirus. *J. Virol.* **88**, 11955–11964 (2014).
29. Abdelnabi, R. et al. A novel druggable interprotomer pocket in the capsid of rhino- and enteroviruses. *PLoS Biol.* **17**, e3000281 (2019).
30. Flatt, J. W., Domanska, A., Seppälä, A. L. & Butcher, S. J. Identification of a conserved virion-stabilizing network inside the interprotomer pocket of enteroviruses. *Commun. Biol.* **4**, 1–8 (2021).
31. Punjani, A., Rubinstein, J. L., Fleet, D. J. & Brubaker, M. A. cryoSPARC: algorithms for rapid unsupervised cryo-EM structure determination. *Nat. Methods*. **14**, 290–296 (2017).
32. Ku, Z. et al. A virus-like particle based bivalent vaccine confers dual protection against enterovirus 71 and coxsackievirus A16 infections in mice. *Vaccine* **32**, 4296–4303 (2014).
33. Hassine, I. H. et al. Characterization of coxsackievirus B4 virus-like particles VLP produced by the Recombinant baculovirus-insect cell system expressing the major capsid protein. *Mol. Biol. Rep.* **47**, 2835–2843 (2020).
34. Dai, W. et al. A virus-like particle vaccine confers protection against enterovirus D68 lethal challenge in mice. *Vaccine* **36**, 653–659 (2018).
35. Zhang, W. et al. A virus-like particle-based tetravalent vaccine for hand, foot, and mouth disease elicits broad and balanced protective immunity. *Emerg. Microbes Infections*. **7**, 91–94 (2018).
36. Nakayama, M. et al. Inhibition of the infectivity of influenza virus by tea polyphenols. *Antiviral Res.* **21**, 289–299 (1993).
37. Chen, X. et al. Intranasal immunization with coxsackievirus A16 virus-like particles confers protection against lethal infection in neonatal mice. *Arch. Virol.* **164**, 2975–2984 (2019).
38. Lin, Y. L. et al. A CpG-adjuvanted intranasal enterovirus 71 vaccine elicits mucosal and systemic immune responses and protects human SCARB2-transgenic mice against lethal challenge. *Sci. Rep.* **8**, 10713 (2018).
39. Tada, R. et al. Enzymatically polymerised polyphenols prepared from various precursors potentiate antigen-specific immune responses in both mucosal and systemic compartments in mice. *PLOS ONE*. **16**, e0246422 (2021).
40. Patel, S. et al. Vitamin A or E and a Catechin synergize as vaccine adjuvant to enhance immune responses in mice by induction of early interleukin-15 but not interleukin-1β responses. *Immunology* **148**, 352–362 (2016).
41. Zheng, Q. et al. Structural basis for the synergistic neutralization of coxsackievirus B1 by a triple-antibody cocktail. *Cell. Host Microbe*. **30**, 1279–1294e6 (2022).
42. Kingston, N. et al. (ed, J.) Production of antigenically stable enterovirus A71 virus-like particles in Pichia pastoris as a vaccine candidate. *The Journal of general virology.* **104**(6), 001867 https://doi.org/10.1099/jgv.0.001867 (2023).
43. Shimizu, T. RNA recognition in toll-like receptor signaling. *Curr. Opin. Struct. Biol.* **88**, 102913 (2024).
44. Hämäläinen, S. et al. Coxsackievirus B1 reveals strain specific differences in plasmacytoid dendritic cell mediated immunogenicity. *J. Med. Virol.* **86**, 1412–1420 (2014).
45. Lei, C., Yang, J., Hu, J. & Sun, X. On the calculation of TCID50 for quantitation of virus infectivity. *Virol. Sin*. **36**, 141–144 (2020).
46. Schindelin, J. et al. Fiji: an open-source platform for biological-image analysis. *Nat. Methods*. **9**, 676–682 (2012).
47. de la Rosa-Trevín, J. M. et al. Scipion: A software framework toward integration, reproducibility and validation in 3D electron microscopy. *J. Struct. Biol.* **195**, 93–99 (2016).
48. Scheres, S. H. W. & RELION Implementation of a bayesian approach to cryo-EM structure determination. *J. Struct. Biol.* **180**, 519–530 (2012).
49. Kimanius, D., Forsberg, B. O., Scheres, S. H. & Lindahl, E. Accelerated cryo-EM structure determination with parallelisation using GPUs in RELION-2. *Elife* 5, e18722 (2016).
50. Zivanov, J. et al. New tools for automated high-resolution cryo-EM structure determination in RELION-3. *eLife* **7**, e42166 (2018).
51. Kimanius, D., Dong, L., Sharov, G., Nakane, T. & Scheres, S. H. W. New tools for automated cryo-EM single-particle analysis in RELION-4.0. *Biochem. J.* **478**, 4169–4185 (2021).
52. Scheres, S. H. W. A bayesian view on Cryo-EM structure determination. *J. Mol. Biol.* **415**, 406–418 (2012).
53. Punjani, A., Zhang, H. & Fleet, D. J. Non-uniform refinement: adaptive regularization improves single-particle cryo-EM reconstruction. *Nat. Methods*. **17**, 1214–1221 (2020).
54. Rosenthal, P. B. & Henderson, R. Optimal determination of particle orientation, absolute hand, and contrast loss in single-particle electron cryomicroscopy. *J. Mol. Biol.* **333**, 721–745 (2003).
55. Pettersen, E. F. et al. UCSF chimerax: structure visualization for researchers, educators, and developers. *Protein Sci.* **30**, 70–82 (2021).
56. Goddard, T. D. et al. UCSF chimerax: meeting modern challenges in visualization and analysis. *Protein Sci.* **27**, 14–25 (2018).
57. Emsley, P., Lohkamp, B., Scott, W. G. & Cowtan, K. Features and development of Coot. *Acta Crystallogr. D Biol. Crystallogr.* **66**, 486–501 (2010).
58. Adams, P. D. et al. PHENIX: a comprehensive Python-based system for macromolecular structure solution. *Acta Crystallogr. D Biol. Crystallogr.* **66**, 213–221 (2010).
59. Chen, V. B. et al. MolProbity: all-atom structure validation for macromolecular crystallography. *Acta Crystallogr. D Biol. Crystallogr.* **66**, 12–21 (2010).
60. Luckow, B. & Lehmann, M. H. A simplified method for Bronchoalveolar lavage in mice by orotracheal intubation avoiding tracheotomy. *Biotechniques* **71**, 534–537 (2021).
61. Diehl, K. H. et al. A good practice guide to the administration of substances and removal of blood, including routes and volumes. *J. Appl. Toxicol.* **21**, 15–23 (2001).

Acknowledgements

We would like to thank Mari Honkanen for training and technical assistance at the Tampere Microscopy Center Facilities (Tampere University). Also, the skillful technical assistance of Ninni Ikonen, Henna-Maarit Kyröläinen and Erja Janhonen is gratefully acknowledged (Virology and Vaccine Immunology Group, Tampere University). We would like to thank Julian Conrad for data collection at the Cryo-EM Swedish National Facility funded by the Knut and Alice Wallenberg, Family Erling Persson and Kempe Foundations, SciLifeLab, Stockholm University and Umeå University. We would like to thank Behnam Lak at the Instruct-ERIC Centre Finland, FINStruct and the Biocenter Finland National CryoEM Facility, and the CSC-IT Center for Science Ltd. for providing technical assistance, sample screening and facilities to carry out the work. Molecular graphics and analyses performed with UCSF ChimeraX, developed by the Resource for Biocomputing, Visualization, and Informatics at the University of California, San Francisco, with support from National Institutes of Health R01-GM129325 and the Office of Cyber Infrastructure and Computational Biology, National Institute of Allergy and Infectious Diseases. This work benefited from access to the cryogenic electron microscopy facility, Helsinki, Finland, an Instruct-ERIC centre. Financial support was provided by Instruct-ERIC (PID: 30128). Figures 2 and 4 utilized Biorender.com. SS discloses support for the research of this work from Tampere University graduate school and Instrumentarium Science Foundation. SG discloses support for the research of this work from Tampere Uni-

versity graduate school, The Research Foundation of the pulmonary diseases and Tampere Tuberculosis Foundation. MJ discloses support for the research of this work from Tampere University graduate school, Tampere Tuberculosis Foundation and Allergy research foundation. VM discloses support for the research of this work from The Jane and Aatos Erkko Foundation (grant numbers 210034 and 240002). SJB discloses support for the research of this work from Research Council of Finland (grant number #315950), The Sigrid Juselius Foundation (grant numbers 95-7202-38 and 121-8570-56) and The Jane and Aatos Erkko Foundation (grant numbers 210034 and 240002). MMH discloses support for the research of this work from Research Council of Finland (grant number #355414) and The Jane and Aatos Erkko Foundation (grant number 240002). The funders played no role in study design, data collection, analysis and interpretation of data, or the writing of this manuscript.

Author contributions

MMH and VM conceived the original idea for the project. MMH and SS developed the idea together into the final research plan. MMH and SS produced, purified and characterized the vaccines. MMH, SS and SG designed the immunological analyses, SS, IM and SG performed immunizations and sampling of the mice. ZP resolved the cryoEM structures with the supervision of SJB. SO provided the sequence for the CVB1-10796 isolate that was used as template for CVB1-VLP. SS, IM and MJ performed ELISA-analyses, MJ and MMH acquired the TEM images. SS, SG, IM, MJ, ML, VM, SJB and MMH analyzed and interpreted results. ZP curated the data. MMH performed DLS-analyses for the study. SS, ZP, SJB and MMH drafted the manuscript and figures. IM produced the graphical abstract under the supervision of SS and MMH. All authors discussed the results and commented on the manuscript. All authors read and approved the final manuscript.

Declarations

Competing interests

The authors declare no competing interests.

Ethics approval and consent to participate

All experiments in this study were carried out following the Finnish Act on the Protection of Animals Used for Scientific or Educational Purposes (497/2013). Procedures were approved by the Regional State Administrative Agency, Pirkanmaa, Finland (decision number ESAVI/1408/2021). All animal reporting was conducted in accordance with ARRIVE guidelines. All efforts were made to minimize animal suffering and to reduce the number of animals used. The welfare of the animals was monitored throughout the experiment.

Additional information

Supplementary Information The online version contains supplementary material available at https://doi.org/10.1038/s41598-025-94656-0.

Correspondence and requests for materials should be addressed to M.M.H.